LBL-10964 c.2
Preprint

Lawrence Berkeley Laboratory
UNIVERSITY OF CALIFORNIA

Physics, Computer Science & Mathematics Division

Submitted to The Astrophysical Journal

LARGE-ANGULAR-SCALE ANISOTROPY IN THE COSMIC BACKGROUND RADIATION

M. V. Gorenstein and G. F. Smoot

May 1980

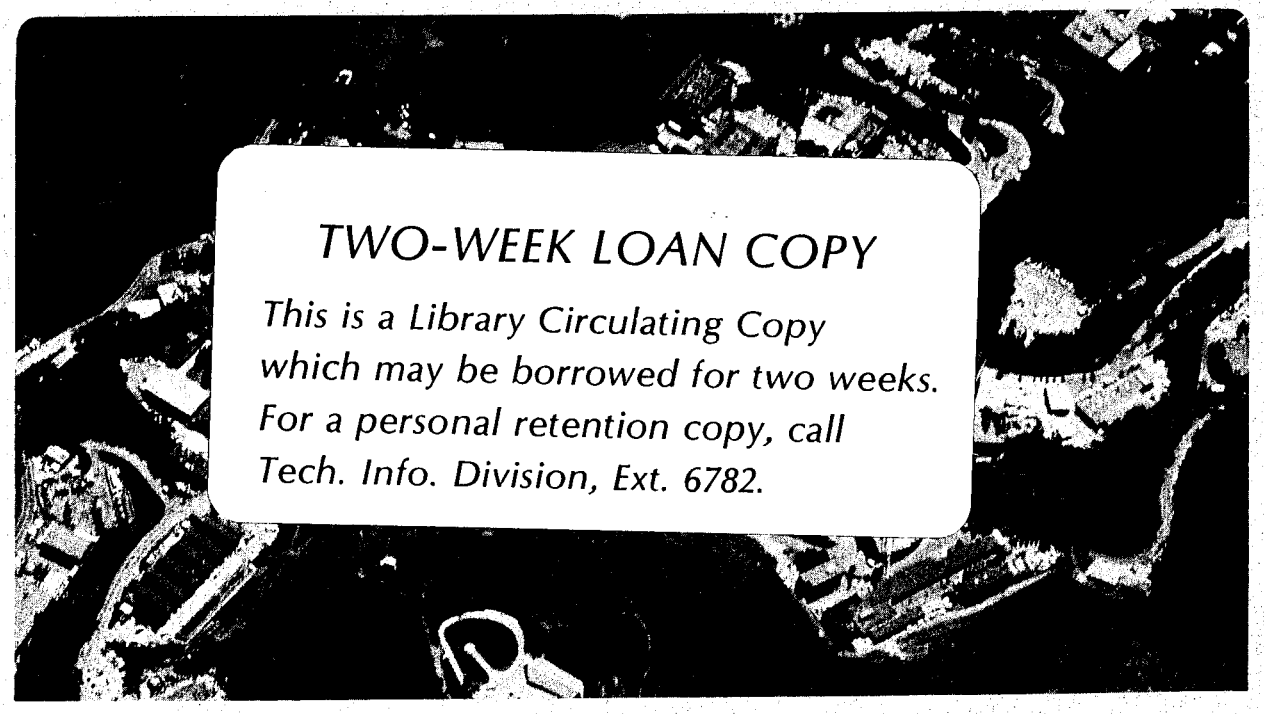

Prepared for the U.S. Department of Energy under Contract W-7405-ENG-48

Subject Heading: *Cosmic Background Radiation — Cosmology*

LARGE-ANGULAR-SCALE ANISOTROPY IN THE COSMIC BACKGROUND RADIATION

M. V. GORENSTEIN and G. F. SMOOT

Space Sciences Laboratory and Lawrence Berkeley Laboratory

University of California, Berkeley California 94720

Received: May 25,1980

ABSTRACT

We report the results of an extended series of airborne measurements of large-angular-scale anisotropy in the 3 K cosmic background radiation. Observations were carried out with a dual-antenna microwave radiometer operating at 33 GHz (0.89 cm wavelength) flown on board a U-2 aircraft to 20 km altitude. In eleven flights, between December 1976 and May 1978, the radiometer measured differential intensity between pairs of directions distributed over most of the northern hemisphere with an rms sensitivity of 47 $mK\ Hz^{-1/2}$. The measurements show clear evidence of anisotropy that is readily interpreted as due to the solar motion relative to the sources of the radiation. The anisotropy is well fit by a first order spherical harmonic of amplitude $360 \pm 50 km\ sec^{-1}$ toward the direction 11.2 ± 0.5 hours of right ascension and 19 ± 8 degrees declination. A simultaneous fit to a combined hypothesis of dipole and quadrupole angular dis-

tributions places a 1 mK limit on the amplitude of most components of quadrupole anisotropy with 90% confidence. Additional analysis places a 0.5 mK limit on uncorrelated fluctuations (sky-roughness) in the 3 K background on an angular scale of the antenna beam width, about 7 degrees.

I. INTRODUCTION

The existence of the cosmic microwave background radiation has profound implications for any theory of the origin and evolution of the universe. Its existence (Penzias and Wilson; 1965) is the strongest evidence we have in support of the hot Big Bang model (Dicke, Peebles, Roll, and Wilkinson, 1965; Weinberg, 1972, pg. 469-609), and its observed isotropy is the strongest evidence we have in support of the Cosmological Principle — the conjecture that the universe is isotropic and homogeneous on a large scale. The properties of the radiation — its spectrum, polarization, and angular distribution — reveal the character of the early universe at an epoch that presumably predates the formation of galaxies.

In the hot Big Bang model, the relic radiation from the primeval fireball has a blackbody spectrum and appears isotropic when measured in a coordinate frame fixed to the general expansion of the universe. An observer moving relative to this frame would measure anisotropy which has an angular distribution described by the Doppler formula (Peebles and Wilkinson, 1968; Peebles, 1971, pg. 147):

$$T(\theta) = T_o \frac{(1-\beta^2)^{1/2}}{(1-\beta\cos\theta)}. \tag{1}$$

For $\beta << 1$, the angular modulation of the radiation temperature approximates a first order spherical harmonic, or dipole anisotropy:

$$T(\theta) \approx T_o(1+\beta\cos\theta) \tag{2}$$

where

$T_o = 3K$ is the mean cosmic radiation temperature.

$\beta = \frac{v}{c}$ is the velocity of the observer.

θ = the angle between the direction of motion and the line of sight.

Peebles (1971) has named this motion the New Aether Drift. The circular motion of the Sun about the galaxy is about 250 km sec^{-1} (Schmidt; 1965) or about one part in 1000 of the velocity of light. The contribution to dipole anisotropy expected from this motion alone is then 3 mK according to Equation 2.

The first precise measurements (Partridge and Wilkinson; 1967) of the large-angular-scale brightness distribution in the microwave background placed limits on dipole and higher order anisotropy at 1 part in 1000 of 3 K at 9.4 GHz (3.2 cm) between directions along the celestial equator. Succeeding measurements at other frequencies placed comparable limits (Boughn, *et. al.*, 1971; Muehlner and Weiss, 1976) or gave ambiguous indication of anisotropy (Conklin; 1969). A balloon-borne measurement by Henry (1971) gave the first evidence of departure from isotropy at 2.9 cm wavelength at one part in 900 of 3 K. Unambiguous detection of *dipole* anisotropy in the cosmic background radiation has now been reported by workers at Princeton (Corey and Wilkinson, 1976; Corey, 1978; Cheng, *et. al.*, 1979) and by our group Smoot, Gorenstein, and Muller, 1977; Smoot and Lubin, 1979). These measurements were carried out with a dual antenna, 33 GHz, microwave radiometer flown to 20 km observation altitude on board a U-2 aircraft.

Our survey of three declination bands in the northern hemisphere finds anisotropy that is well fit by a dipole distribution of amplitude 3.6 ± 0.5 mK, with the axis of symmetry pointing toward (11.2 ± 0.5 hrs. R.A., $19^\circ \pm 8^\circ$ dec.) or ($l^{II} = 229^\circ \pm 19^\circ, b^{II} = 66^\circ \pm 7^\circ$). The data place limits of 1 mK on most components of anisotropy described by a quadrupole distribution, and limits of 0.5 mK on "sky-roughness" on an angular scale of 7° set by the beamwidth of the antennas. The lack of higher order anisotropy places new limits on processes of cosmological interest, while the detected dipole anisotropy is readily interpreted as due to the motion of the sun relative to the last-scatterers of the microwave background. For a background temperature of 3 K, 3.6 mK corresponds to a velocity of 360 $km\ sec^{-1}$. Subtracting the 250 $km\ sec^{-1}$ circular motion of the sun about the Milky Way Galaxy from the microwave velocity yields the Galaxy's motion relative to the background. Surprisingly, the velocity is large, in excess of 500 $km\ sec^{-1}$ and points within 33° of the Virgo Cluster of Galaxies.

This paper elaborates and extends the preliminary announcement (Smoot, *et. al.;* 1977) of our result. In that Letter we combined data from four flights, where the equipment was undergoing development, together with data from four additional flights, when the equipment was in

its final configuration. Three flights subsequent to that publication have extended the sky coverage in the northern hemisphere as summarized in Table 1. Thus, seven flights altogether (#8 - 14) collected data with the equipment in its final configuration and form the subset of data we concentrate on here.

This paper tabulates the collected data and describes its acquisition, calibration, and the corrections made to it for systematic backgrounds. In addition, it describes the data analysis and presents the astrophysical interpretation of these results. The detailed description of the equipment and its design is presented elsewhere (Gorenstein, Muller, Smoot, and Tyson; 1978). We emphasize that the observational apparatus and data taking strategy were carefully designed to cancel or reduce the effects of known systematic backgrounds; the resulting corrections to the data are small compared to the size of the signal.

The 33 GHz airborne radiometer has recently completed a series of anisotropy observations in the southern hemisphere (Smoot and Lubin; 1979) complementing the more extensive northern hemisphere observations discussed in detail here. This new data has independently confirmed the direction and magnitude of dipole anisotropy, and together with the northern hemisphere data has placed sub-milli-Kelvin limits on all components of quadrupole anisotropy in the microwave background radiation.

This paper's organization is as follows. Section II briefly reviews the equipment operation and design, and describes the data taking procedures and reduction techniques. Appendix A documents the calibration procedures used to convert anisotropy measured in empirical units to milli-Kelvin, and Appendix B details the corrections applied to the reduced data for instrumental, atmospheric, and astrophysical backgrounds. Section III presents the tabulation of the reduced measurements of anisotropy taken in the northern hemisphere. Section IV concentrates on the statistical analysis that extracts the estimates of dipole parameters and the limits on higher order anisotropy from these measurements. Section V interprets the results due to the motion of the earth, compares this microwave velocity with other measurements of galactic motions, and discusses the significance of the limits on higher order anisotropy. Section VI

concludes this work with a summary of the results, the limitations of this measurement, and future directions for measurement of anisotropy.

II. DESCRIPTION OF THE APPARATUS AND EXPERIMENT

a) The Instrument

A schematic diagram of the twin-antenna Dicke radiometer used in these measurements is shown in Figure 1. The equipment is discussed in detail elsewhere (Gorenstein, Muller, Smoot, and Tyson; 1978). Here we summarize the crucial design features.

Observations are carried out with the radiometer mounted on board a U-2 aircraft flown to 20 km altitude. The radiometer, operating at 33 GHz (9 mm), measures the difference in incoming power, with an rms sensitivity of 47 $mK\ Hz^{-1/2}$ between the two antennas pointed 60° apart in the sky. Atmospheric and galactic microwave emissions are potentially serious backgrounds to a sensitive anisotropy experiment. The 20 km altitude and the 33 GHz frequency reduce these spurious signals, external to the apparatus, below 0.2 mK. The antennas, pointing 30° from the zenith, receive a 60 mK contribution to antenna temperature from atmospheric constituents, primarily from O_2 emission. Pointing both antennas 30° from the zenith cancels this residual emission below 0.1 mK for level flight of the U-2.

The intensity of galactic synchrotron emission falls below 1 mK above about 30 GHz. At 33 GHz the corrections to the data due to anisotropic galactic synchrotron emission are barely significant — less than 0.2 mK.

A hierarchy of switchings and reversals detects and eliminates spurious signals intrinsic to the equipment. Rapid switching (100 Hz) between the two antennas eliminates the effects of gain fluctuations (1/f noise) in the receiver. Insertion loss imbalance between the radiometer

arms ($\approx$60 mK) is canceled by rotating the apparatus 180° about the vertical every 64 seconds, interchanging the two antennas. Spurious constant anisotropies associated with the rotation state are eliminated by reversing the flight path of the aircraft every 20 minutes.

The experiment incorporates additional features that reveal or cancel systematic effects to well below the milli-Kelvin level. The equipment is shielded against radio-frequency interference and magnetic fields. The entire apparatus is thermally regulated with special regard for critical components. The antenna's design combines low insertion loss with low sidelobe gain. The meausured gain in the direction of the earth is less than 10^{-7} of the forward direction (Janssen, *et. al.;* 1979). The antennas point symmetrically to the pilot's left and right, 180° apart in azimuth, and 30° from the zenith, thereby cancelling the bulk of the emission from the earth and aircraft. Residual anisotropic emission from the earth and aircraft are estimated to be less than 0.3 mK. A second twin-antenna radiometer operating at 54 GHz monitors and eliminates anisotropic atmospheric emission. This monitor showed that the autopilot maintained level flight during data taking to better than 0.2° of bank, and that the resulting spurious signal at 33 GHz from the aircraft tilt was less than 0.2 mK. The data and housekeeping information are digitized and recorded on magnetic cassette on board the aircraft.

A radiometer conveniently measures brightness, B (ergs/sec cm^2 Hz ster), about a fixed observation frequency, ν. The relation between brightness and radiation temperature, T, for a thermal spectrum is given by the familiar Planck distribution,

$$B(\nu)=kT\frac{2\nu^2}{c^2}\frac{x}{e^x-1} \tag{3}$$

where

k = Boltzmann's constant.

h = Planck's constant.

c = the velocity of light.

$x = h\nu/kT$.

An observed differential variation in brightness, δB, then corresponds to variation in radi-

ation temperature, δT, given by,

$$\delta B(\nu) = k\delta T \frac{2\nu^2}{c^2} \frac{x^2 e^x}{(e^x - 1)^2}. \tag{4}$$

For high temperatures and low frequencies, where x is much less than one, equation (3) reduces to a linear relation between brightness and radiation temperature,

$$B(\nu) = 2kT \frac{\nu^2}{c^2} \tag{5}$$

and we can re-express the brightness in thermal units by defining the brightness or antenna temperature to be,

$$T_{antenna} = \frac{B(\nu)}{2k} \frac{c^2}{\nu^2}. \tag{6}$$

The antenna temperature equals the thermal temperature of a source if that source fills the antenna beam and emits like a blackbody at the observation frequency, and if observation frequency is in the low-frequency Rayleigh-Jeans part of the spectrum.

Combining equations (4) and (6) we arrive at the antenna temperature variation for a variation in radiation temperature of a thermal source,

$$\delta T_{antenna} = \delta T \frac{x^2 e^x}{(e^x - 1)^2}. \tag{7}$$

For ν = 33 GHz, and T = 3 K, x = 0.53, and $\delta T = 1.023\ \delta T_{antenna}$.

Throughout this paper, we assume that the cosmic background radiation follows a Planck spectrum of temperature 3 K near 33 GHz.

b) Data Acquisition

The data reported here were accumulated in eleven flights made between December 1976 and May 1978. Figure 2 shows the total sky coverage. After deletion of data taken during periods of ascent, descent, antenna rotation, and aircraft banks, a typical 4.75 hour flight yields about 3.5 hours of data taken at altitude. All flights described here originated and ended at Moffett Field, California (+38° north latitude and 122° west longitude).

A typical flight plan is organized into 12 paths of straight-and-level flight, each of about 20 minutes duration. One 20 minute flight path effectively measures the temperature difference

between two points on the sky to an accuracy of 1.6 mK rms. In 20 minutes the combination of earth's rotation and the aircraft's 740 km hr velocity sweep the antennas' beams from 2 to 5 degrees across the celestial sphere. This swath is less than the 7° beam width (FWHM) of the antennas, so little angular resolution is lost in averaging all data from a single path.

In a typical flight, six initial paths are flown with alternating east-west headings, measuring anisotropy between regions of the sky separated 60° in declination but with essentially the same right ascension. The six final paths are flown with alternating north-south headings, measuring anisotropy between regions of the sky separated along right ascension but with the same declination. Paths flown in pairs with opposing headings cancel systematic effects intrinsic to the rotation state of the system.

Flights usually begin with a sunset launch. The combination of ascent and a 20 minute initial flight path at altitude provides a 30 minute period in the cold atmosphere during which the equipment reaches thermal stability prior to data-taking. Several of the flights included flight paths which pointed one antenna directly at the moon for a few minutes checking the absolute calibration of the 33 GHz radiometer. Flight paths accumulating anisotropy data were designed to avoid the moon and the galactic plane (particularly the intense Cygnus X region).

c) Data Reduction

During flight, the on-board data recording system integrates the analog signal every two seconds and records it in digital form on a cassette tape. Post-flight analysis commences with the transfer of these digitized data, together with housekeeping information, from cassette to a standard computer tape. Computer programs produce plots of the data and housekeeping signals as a function of time, and correlate the data with the actual flight plan.

After preliminary inspection, editing programs retain only the data recorded at altitude when the antennas were properly oriented. Data are automatically deleted if taken just before, during, or after antenna rotation: this selection retains 56 seconds in each 64 second antenna rotation half-cycle. Data are also deleted if the aircraft departs more than one degree from

counter-clockwise antenna orientations for the phase switch states of 0° and 180° .

A celestial anisotropy appears as a signal alternating in phase with the rotation of the antennas. If there are no other (spurious) signals that also interchange with the antenna rotation, then the subtraction of the mean signals recorded in each antenna orientation correctly extracts the celestial anisotropy from the data. However, internal signals synchronous with the antenna rotation can contribute to the anisotropy signal from each flight path. We call such a signal a rotation offset to distinguish it from the fixed intrinsic offset between the radiometer inputs. While the intrinsic offset is detected with the phase switching and cancelled with the antenna rotation, the rotation offset is detected and cancelled with the alternation of the aircraft heading.

The rotation offset present in the accumulated data is typically 2 mK and stable throughout a given flight to about ± 0.5 mK. Its subtraction from the data prior to the fitting changes none of the astrophysical results. The detailed nature of the offset and its possible origins is the subject of Appendix B *(f)*.

Averaging the differenced data reduces the rms noise fluctuations by $t^{-1/2}$, where t is the integration time. The radiometer has a sensitivity of 47 $mK\ Hz^{-1/2}$, data from a 20 minute path yields a measurement with an rms uncertainty of about $\pm$ 1.6 mK.

level flight as indicated by the 54 GHz roll monitor. The edited data are re-plotted as a function of time, and inspected for spurious signals. In the 35 hours of data accumulated from eleven flights, only two 20 second deletions were required to eliminate spikes in the 33 GHz signal that are inconsistent with the measured receiver noise.

Differencing the averaged 33 GHz signal recorded when the antennas are oriented clockwise (CW) from when the antennas are oriented counter-clockwise (CCW) eliminates the intrinsic imbalance in the radiometer. An intrinsic imbalance will produce a non-zero output signal when no differential input signal is present. Insertion loss difference between the two circulation directions of the ferrite switch dominates the intrinsic imbalance. A low intrinsic imbalance minimizes spurious fluctuations in signal level arising from small gain changes in the radiometer system. Laboratory adjustment of insertion loss stubs incorporated in each input port of the switch reduces a 1 K offset to less than 60 mK.

A slight modification to the standard Dicke switch configuration allows us to monitor the intrinsic imbalance throughout the flight. We include a switch that reverses the sign of 100 Hz demodulation waveform every 12 seconds. Since this is equivalent to changing phase by 180°, we call this feature the 180° phase switch. The mean difference between signals recorded in each phase state measures the amplitude of the 100 Hz waveform resulting from the upstream imbalance between radiometer inputs.

The combination of antenna reversal and phase switching yields four sets of data based on the antenna orientation and phase state. The following expressions illustrate the way in which an external signal is extracted from averages of data taken in the individual states:

$$\Delta T_{anisotropy} = \frac{\left[\left(\frac{\Delta T_{CW} - \Delta T_{CCW}}{2}\right)_{0^\circ} - \left(\frac{\Delta T_{CW} - \Delta T_{CCW}}{2}\right)_{180^\circ}\right]}{2} \qquad (8a)$$

$$\Delta T_{offset} = \frac{\left[\left(\frac{\Delta T_{CW} + \Delta T_{CCW}}{2}\right)_{0^\circ} - \left(\frac{\Delta T_{CW} + \Delta T_{CCW}}{2}\right)_{180^\circ}\right]}{2} \qquad (8b)$$

where ΔT_{CW} and ΔT_{CCW} are the mean of the 33 GHz data as recorded in the clockwise and

III. THE REDUCED MEASUREMENTS OF ANISOTROPY

Table 2 lists 106 measurements of anisotropy collected from flights 4 through 14. Each entry is the average of data taken in a flight path that measured anisotropy between directions in the sky 60° apart. The sign convention is:

$$\Delta T_{3K} = T(\hat{n}_R) - T(\hat{n}_L) \tag{9}$$

where $T(\hat{n})$ is the temperature of the background radiation in the $\hat{n}$ direction and ΔT_{3K} measures the anisotropy between $\hat{n}_R$ and $\hat{n}_L$. The antenna on the pilot's right points towards $\hat{n}_R$, and the antenna on the pilot's left points towards $\hat{n}_L$.

Two cross-checks verify the sense of the sign. Aircraft banks cause imbalance in atmospheric emission into the horn antennas so the schedule of right and left banks in the flight plan produces a succession of positive and negative test signals of known magnitude and sign. A three minute bank at 20° roll angle yields a 24 ± 4 mK signal at 33 GHz. A right bank yields a positive atmospheric signal in the sense of Equation (9), since $\hat{n}_R$ points towards the horizon through a greater atmospheric optical depth. As a second check, the moon, viewed in the southern sky by one antenna of the radiometer, yields a positive signal when the aircraft heads in an eastward direction.

Flights 8 through 14 were flown with the single best receiver system and with the equipment in unchanged configuration. These flights had almost complete coverage in right ascension in three declination bands: +7°, +37° and +67°, reflecting the choice of flight paths with alternated north-south and east-west headings. In-flight measurements of system noise temperature, rms noise fluctuations, insertion loss offset, and physical temperatures of critical components show that the equipment performance was sufficiently similar in all flights that we treat the data in a consistent manner throughout. For example, for these flights we use the same calibration constant to convert data measured in empirical units to milli-Kelvin.

The errors listed in Table 2 are the one-standard-deviation uncertainties in the corresponding measurement. These values are statistical only and are scaled from the rms fluctuations computed from the meaurements of anisotropy recorded every two seconds

throughout a flight path. In flights 8-14 these rms fluctuations measure the receiver sensitivity to be $47 \pm 2\ mK\ Hz^{-1/2}$. Thus data integrated for 20 minutes measures anisotropy with an rms error of about 1.6 mK. The empirically determined value for receiver sensitivity agrees with the *a priori* value predicted from the radiometer equation (Kraus; 1966, pg. 258):

$$\delta T_{rms} = \frac{k\ T_s}{\sqrt{B\ T}} \tag{10}$$

where

δT_{rms} = the rms error.

T_s = the system temperature.

B = the i.f. bandwidth.

t = the integration time.

k = a constant factor for a Dicke radiometer utilizing square-wave modulation and sine-wave multiplication $k = \pi/\sqrt{2} \approx 2.22$.

With the values measured in the laboratory for the receiver used in flights 8-14 ($T_s = 600 \pm 50\ K,\ B = 500 \pm 20\ MHz$), equation (10) gives $\delta T_{rms} = 46 \pm 5\ mK\ Hz^{-1/2}$. (During a flight path, the contribution to rms fluctuations from atmospheric, galactic, or thermal backgrounds, or changes in instrumental offset are all expected to be neligible compared to the integrated 1.6 mK receiver noise.) Auto-correlation of the data recorded in each flight path yields no evidence for correlation between data recorded after each two second integration. The distribution of the data about their mean has been checked for each flight path and found consistent with the expected Gaussian distribution.

During flight 10, two 500 mK spikes inconsistent with radiometer noise required the deletion of 40 seconds of data. This was the only instance where inspection of the 33 GHz signal revealed a spurious signal of unknown origin. The data collected in the first 6 flight paths of flight 10 are not presented here because the thermal sensors in the antennas indicated that the equipment had not come to thermal stability. For this flight, the sun was still above the horizon for the first few flight paths, and the heated antenna surfaces could have injected a

spurious signal of a few milli-Kelvin.

As described in Appendix B, *(f)*. there is a rotation offset signal of about two milli-Kelvin present in the data, probably due to an asymmetry in the instrument between antenna rotation orientations. The once-per-twenty minutes alternation of aircraft headings measures this offset, and we have subtracted the mean offset for each flight from the data prior to tabulation in Table 2. The subtraction of a constant offset changes none of the conclusions drawn from the astrophysical analysis of the data, but allows us to treat measurements from each flight path as deviations from isotropy.

IV. INTERPRETATION OF MEASUREMENTS AS ANISOTROPIES

This section presents the results from the statistical analysis of the data collected in flights 8-14. The data are inconsistent with an isotropic background, their scatter implying anisotropy on a large angular-scale in the cosmic background of about one part in 1000 of 3 K. The first order spherical harmonic (dipole) model accounts satisfactorily for this anisotropy. As shown in sub-section *(b)*, the best-fit dipole has an amplitude of 3.6 $\pm$ 0.5 mK with post-fit residuals consistent with the *a priori* estimates of receiver noise. The chi-squared for the fit is 71.0 for 73 degrees of freedom and yields a confidence level of 55%. No measurements deviate by an amount inconsistent with receiver noise from the best-fit dipole. At the present level of sensitivity the data requires no further angular distribution in addition to the dipole model. We compare the dipole anisotropy found here with other measurements of microwave anisotropy on a large-angular scale. A dipole anisotropy of about 3 mK is anticipated due to the sun's motion about the Milky Way Galaxy. Surprisingly, the observed anisotropy points away from this rotational motion. We leave to section V the comparison of the dipole anisotropy to other all-sky measurements of local motion.

Since the data samples the sky extensively in right ascension we can unambiguously distinguish between dipole anisotropy and a possible second order spherical harmonic (quadrupole) anisotropy varying along the celestial equator. In subsection *(c)* we show that the data places limits of less than 1 mK on these components of quadrupole anisotropy. In subsection *(d)* we show that "sky-roughness" in the 3 K background on an angular scale of 7° set by the antenna beam size is less than 0.5 mK.

a) The Dipole Anisotropy - First Order Spherical Harmonic

The following expression describes a dipole anisotropy in the 3 K background radiation

$$T(\hat{n}) = T_0 + \vec{T}\cdot\hat{n} \tag{11}$$

where

$T(\hat{n})$ is the radiation temperature in the direction $\hat{n}$.

$\vec{T}$ is the amplitude and direction of the dipole anisotropy.

T_0 is the mean temperature, not measured in this experiment.

Since the 33-GHz radiometer measures the *difference* in temperature between two directions, $\hat{n}_R$ and $\hat{n}_L$, the following equation models dipole anisotropy for the data:

$$\Delta T(\hat{n}_R,\hat{n}_L) \equiv T(\hat{n}_R) - T(\hat{n}_L) = \vec{T}\cdot(\hat{n}_R - \hat{n}_L). \tag{12}$$

Minimizing the sum of the weighted, squared deviations of the dipole model from the data in Table 2, flights 8-14, determines $\vec{T}$ to be

$$|\vec{T}| = 3.6 \pm 0.4\, mK \tag{13a}$$

$$\hat{T} = 11.2 \pm 0.4 \text{ hours R.A., } 19^{\circ} \pm 6^{\circ} \text{ dec.} \tag{13b}$$

The unit vector $\hat{T}$ points towards the "hotter" hemisphere. The errors quoted are statistical only. Table 3 summarizes the parameters that model dipole anisotropy in the data together with their errors and correlation coefficients. These parameters are expressed in celestial coordinates, galactic coordinates, rectangular celestial coordinates, and finally in the rectangular diagonal coordinates that have uncorrelated errors. Errors expressed in rectangular coordinates have a Gaussian distribution. The errors on all parameters listed in this table are 25% larger than the statistical errors; the increase accounts for uncertainty in terrestrial emission into the antenna sidelobes, as discussed in Appendix B *(c)*.

Column (10) in Table 2 lists each measurement's contribution to chi-squared computed for the best fit dipole parameters. The value of chi-squared computed for the fit is 71.0 for 73 degrees of freedom, corresponding to a confidence level of about 55%. Figure 3 plots ΔT^i_{3K} versus the angle between $\vec{T}$ and the difference vector $(\hat{n}^i_R - \hat{n}^i_L)$ for the i^{th} measurement. The

curved line represents the dipole anisotropy drawn in for comparison. In contrast to the dipole anisotropy, the horizontal line, $\Delta T = 0$, gives a poor fit to the data. The value of chi-squared for this null hypothesis is 171, and gives a confidence level, for 76 degrees of freedom, of less than 10^{-9}.

Figure 4 is a sky map of the galactic backgrounds extrapolated from sky maps made at lower frequencies as outlined in Appendix B *(a)*. Brightness is represented by antenna temperature at 33 GHz and is projected on the third axis. The sky coverage in flights 4-14, Figure 2, compared to the galactic backgrounds, graphically demonstrates the minimal contamination introduced by galactic backgrounds into the observed dipole anisotropy.

Table 3 summarized the analysis for dipole anisotropy on the set of data taken with the best receiver and with the equipment in unchanged configuration. Table 4 presents the results for fits to subsets of this data, and to selections that include measurements from earlier flights. The quoted errors in this table are statistical only. The results demonstrate the internal consistency of the data.

Table 5 compares other microwave measurements of dipole anisotropy with the results from this work. Cheng, *et al.* (1979), Corey (1978), and Henry (1971) each employed balloon-borne platforms and collected their data with twin-antenna radiometers. Column (1) references the measurements, and column (2) lists the observation frequencies. Columns (3), (4), and (5) list the parameters and errors of dipole anisotropy expressed in celestial coordinates. Columns (6), (7), and (8) express the parameters and errors in rectangular coordinates with the correlation coefficients listed in columns (9), (10), and (11).

The measurements are all in rough agreement. Our measurement at 33.0 GHz and the Cheng, *et al.* measurement at 31.4 GHz have the smallest errors. Also the Cheng, *et al.* 31.4 GHz measurement, by being their highest frequency, will be least affected by corrections due to galactic synchrotron emission. We compare these two measurements by computing the difference vector and correlated errors. We find the difference vector to have a magnitude of 1.8 mK, and from the combined error matrices compute a chi-squared of 7.5 for three degrees

of freedom. The probability of measuring a difference magnitude of 1.8 mK or more is then 6%, indicating a marginal disagreement. Discrepancies may be due to unknown systematic effects, unaccounted for sources of celestial anisotropy, or underestimation of errors by about $\sqrt{7.5/3}$, or a factor of 1.6.

b) Analysis of Quadrupole Anisotropy - Second Order Spherical Harmonic

One of the reasons for investigating angular variations in the 3 K background radiation is to search for higher order multipoles in $T(\hat{n})$. The existence of multipole anisotropies higher than dipole would present a challenge to the Cosmological Principle. We have analyzed the data for evidence of a quadrupole anisotropy.

The quadrupole distribution, $Q(\hat{n})$, if formed from a linear combination of five basis functions, $q_i(\hat{n})$,

$$Q(\hat{n}) \equiv \sum_{i=1}^{5} Q_i q_i(\hat{n}) \tag{14}$$

Table 6 defines the basis functions in terms of the second order, $l = 2$ spherical harmonics. The five parameters, Q_i, represent the amplitudes of quadrupole anisotropy expressed in milli-Kelvins. The combination of $Q(\hat{n})$ with the dipole distribution, equation (5), models the observed sky temperature as the sum of dipole plus quadrupole anisotropy; thus,

$$T(\hat{n}) = T_o + \vec{T}\cdot\hat{n} + Q(\hat{n}). \tag{15}$$

Minimizing the following expression for chi-squared yields the least-squares estimate for the three dipole and five quadrupole parameters:

$$\chi^2 = \sum_{i=1}^{M} \frac{[\Delta T_{3K}^i - \vec{T}\cdot(\hat{n}_R^i - \hat{n}_L^i) - (Q(\hat{n}_R^i) - Q(\hat{n}_L^i))]^2}{\sigma_i^2} \tag{16}$$

The index i is summed over differential measurements of anisotropy $\Delta T_3 K^i$ between directions $\hat{n}_R$ and $\hat{n}_L$. The quantity σ_i^2 is the *a priori* variance for each measurement, scaled from the rms fluctuations due to receiver noise.

Table 7 presents the results to a fit based on the eight parameter hypothesis. It is worthwhile to compare the dipole parameters in Table 3 with the dipole parameters listed in

Table 7. For the dipole fit alone, $T_{\hat{x}}$ has a value of $-3.3 \pm 0.4\,mK$. In the combined fit of dipole with quadrupole moment, the $T_{\hat{x}}$ parameter retains its significance in the presence of the competing quadrupole hypothesis, with a value of $-2.3 \pm 0.7 mK$. This is evidence that the major component of global anisotropy is correctly interpreted as a dipole signal, and cannot be due to a quadrupole signal from a partially surveyed sky.

The Q_i parameters do not indicate the presence of quadrupole anisotropy:

(1) The values of the parameters Q_i listed in Table 7 are consistent with zero. (The large correlated errors in Q_1 and T_z will be explained presently as due to restricted sky coverage.)

(2) The value of χ^2 for the eight parameter fit is 62.6 compared to $\chi^2 = 71.0$ for the fit to the three parameter dipole hypothesis alone. This demonstrates, without reference to a particular parametrization, that the inclusion of the quadrupole hypothesis is not required by the data. The *change* in χ^2 between these fits is distributed as χ^2 for five degrees of freedom *if* the quadrupole amplitudes have zero mean (Martin, 1971, pg. 146). Since the confidence level for an χ^2 of 8.4 with five DOF is 15%, we conclude that the data are consistent with zero mean quadrupole amplitude.

It is natural to ask what limit the data places on quadrupole anisotropy in the cosmic background radiation. All data flights were flown from Moffett Field, CA, 37° north latitude. The consequences of restricted flight latitude is that the measurements cannot distinguish between a $\sin\delta$ distribution (polar component of dipole) and a $\frac{3}{2}\sin^2\delta - \frac{1}{2}$ distribution (polar axially symmetric component of quadrupole). Because the anisotropy measurements are differential, both distributions have identical cosinusoidal variation dependent on aircraft heading alone (Brian Corey, private communication): Thus observations at fixed latitude yield only a weighted average of T_z and Q_1, with the consequence that the estimated values of these parameters have large correlated errors. Despite the correlation between Q_1 and T_z the data does place a significant limit on the remaining four quadrupole amplitudes. We express this limit as the rms

amplitude of a quadrupole distribution, defined as

$$Q \equiv \left[\frac{1}{4\pi}\int\int Q^2(\hat{n})\, d\Omega\right]^{1/2} = \left[\frac{1}{5}Q_1^2+\frac{4}{15}\sum_{i=2}^{5} Q_i^2\right]^{1/2} \tag{17}$$

Restricting ourselves to the four basis functions determined with good sensitivity, we define Q' as

$$Q' \equiv \frac{2}{\sqrt{15}}\left[\sum_{i=2}^{5} Q_i^2\right]^{1/2} \tag{18}$$

The data from Table 7 give

$$Q'_{data} = 0.6mK \tag{19}$$

A Monte-Carlo simulation generates the distribution of Q' by adding independent error signals to each flight path-measurement simulating the effect of receiver noise. In 90% of the cases, Q' is less than 1.1 mK, thus we place an upper limit on quadrupole anisotropy of one part in 3000 of 3 K, at a confidence level of 90%.

c) Limit on Sky-Roughness on a 7° Angular Scale

The excellent agreement of the data with the simple dipole model allows us to place limits on higher order anisotropy. Such anisotropy may result from fluctuations in the primordal plasma positively related to galaxy formation subsequent to the epoch of decoupling.

We determine limits on fluctuations in the temperature of the cosmic background on an angular scale set by the antenna beam width, about 7°. We assume σ_s is the rms amplitude of sky roughness in any one direction, and that such fluctuations are uncorrelated between directions separated by more than about 60° in the sky, an angle set by the separation of the two antenna beams. Then the temperature differences measured should fluctuate in an uncorrelated way by $\sqrt{2}\sigma_s$ about the best fit dipole anisotropy.

The data recorded in a single flight-path determines the rms amplitude due to receiver noise alone to be about 1.6 mK. The good agreement of the rms deviations of the post-fit residuals for the dipole model with this *a priori* estimate of receiver noise indicates that possible sky-roughness is small compared to 1.6 mK. A hypothesized sky-roughness, σ_s, of 0.5 mK

would imply a confidence level of 90% for the dipole fit, as contrasted to 55% if σ_s were hypothesized (as usual) to be zero. We then interpret this as an upper limit. level on sky-roughness, averaged over 7° patches, at one part in 6000 of 3 K. This analysis places a sensitive limit in the angular range intermediate between large-angular-scale measurements (such as this experiment was primarily designed for) and arc-minute-scale measurements conducted with large parabolic antennas (see for example Conklin and Bracewell, 1967; and Birkinshaw, *et. al.*, 1978).

V. ASTROPHYSICAL INTERPRETATION

We assume the conventional view that the dipole anisotropy in the microwave background radiation identifies the local frame at rest with respect to the sources — or last scatterers — of the 3 K radiation. Similarly we interpret limits on higher order anisotropy as constraints on the parameters of cosmological models describing the evolution of the early universe. In subsection *(a)* we find the velocity of the Local Group of galaxies with respect to the 3 K background radiation to be large, $545 \pm 43\ km\ sec^{-1}$. We compare this with velocities of the Local Group measured relative to galactic clusters and selected sets of galaxies. In subsection *(b)* we comment on the cosmological implications from the limits on quadrupole anisotropy and medium scale sky roughness.

(a) The Motion of the Sun and Nearby Groups of Galaxies Relative to the 3 K Background Radiation

Given the magnitude of the measured dipole anisotropy $|\vec{T}|$ the following expression from Eq. (2) gives the magnitude of velocity $|\vec{V}|$ relative to an isotropic thermal background radiation of temperature T_o:

$$|\vec{V}| = \frac{|\vec{T}|}{T_o}\, c \ ; \ |\vec{T}| << T_o \tag{20}$$

where c is the velocity of light. Thus from the data in Table 3 we arrive at,

$$|\vec{V}| = \frac{(3.61 \pm 0.54) \times 10^{-3}\, K}{3.0\, K}\left[\frac{3.0\, K}{T_o}\right] \times (3 \times 10^5 km\ sec^{-1}) \tag{21}$$

$$= (361 \pm 54) \times \left[\frac{3.0\, K}{T_o}\right] km\ sec^{-1}.$$

For a radiation temperature T_o of 3 K, a dipole anisotropy of 1 mK corresponds to a velocity of

$100\,km\ sec^{-1}$.

Recent measurements (Woody and Richards; 1979) suggest that the spectrum of the background radiation may deviate from the Planck distribution at sub-millimeter wavelengths. Even so, motion will still yield a cosine modulation in the brightness temperature of an otherwise isotropic background radiation. The relation between an observer's velocity and the modulation amplitude depends on the distribution's spectral index at the observation frequency, ν_0, such that if the spectral brightness ($ergs\ sec^{-1}cm^{-2}ster^{-1}Hz^{-1}$) is given by:

$$B(\nu) = B_0(\frac{\nu}{\nu_0})^{\alpha}, \tag{22}$$

where α is the spectral index of the (distorted) spectrum, then for non-relativistic velocities β, the directionally dependent brightness $B(\theta)$, is given by (Compton and Getting, 1935; Schwartz,1970):

$$B(\theta) = B_0[1 + (3-\alpha)\,\beta\cos\theta]. \tag{23}$$

For an amplitude of dipole anisotropy ΔB, measured by the observer, the observer's motion is then inferred to be:

$$\beta = \Delta\frac{B}{B_0}\frac{1}{3} - \alpha\,. \tag{24}$$

In the Rayleigh-Jeans region of a Planck distribution, $\alpha = 2$, and we recover the results of Eq. (2). We assume a Planckian distribution in the following discussion.

We now find the motion of the Local Group relative to the microwave background, by subtracting the motion of the sun with respect to the members of the Local Group from the motion of the sun with respect to the background radiation. Yahil *et. al.*, (1977) have made a recent re-determination of the motion of the sun with respect to eleven galaxies in the Local Group whose peculiar motions dominate the effects of the Hubble expansion. Yahil *et. al.*, (1977) find a velocity of the sun with respect to the centroid of these galaxies to be $302 \pm 22 km\ sec^{-1}$ toward $l^{II} = 105^{\circ} \pm 5^{\circ}$, and $b^{II} = -7^{\circ} \pm 4^{\circ}$, a value close to the "standard" vector of $300\,km\ sec^{-1}$ toward $l^{II} = 90^{\circ}$, $b^{II} = 0^{\circ}$. The Galaxy itself appears nearly stationary with respect to the Local Group (de Vaucouleurs and Peters, 1968; de Vaucouleurs, 1972;

Yahil, Tammann, and Sandage, 1977) as the observed redshifts of the members of the Local Group are nearly accounted for by the 250 $km\ sec^{-1}$ circular motion of the sun about the Milky Way toward $l^{II}=90^{o}$, $b^{II}=0^{o}$ (Schmidt;1965).

Table 8 presents the motion of the sun with respect to the 3 K radiation inferred from the dipole anisotropy, the motion of the sun with respect to the centroid of the eleven galactic members of the Local Group (Yahil, *et. al.*, 1977; solution 2), and the combination of these velocities that yields the motion of the Local Group with respect to the microwave background. Column (1) references the measurements, columns (2), (3), and (4) list the velocities expressed in galactic coordinates with rms errors. Columns (5), (6), and (7) list the components in rectangular coordinates where $\hat{X}$ points toward the galactic center ($l^{II}=0^{o}, b^{II}=0^{o}$), $\hat{Y}$ points toward the local direction of the galaxy's rotation ($l^{II}=90^{o}, b^{II}=0^{o}$), and $\hat{Z}$ points toward the north galactic pole ($b^{II}=+90^{o}$). Columns (8), (9), and (10) list the correlation coefficients for the rectangular parameters. In the last row of Table 8, we re-express the motion of the Local Group in the supergalactic coordinates (L,B) of de Vaucouleurs *et. al.*, (1976). The peculiar motion of the Local Group relative to the 3 K radiation is large, $545 \pm 43\ km\ sec^{-1}$, toward $l^{II}=268^{o} \pm 7^{o}$, $b^{II}=42^{o} \pm 7^{o}$ or $L = 123^{o} \pm 7^{o}$; $B = -29^{o} \pm 7^{o}$. It is interesting that the direction of motion of the Local Group points within $33^{o} \pm 7^{o}$ of the Virgo cluster of galaxies ($l^{II}=280^{o}$, $b=75^{o}$; $L = 102^{o}$, $B = -3^{o}$) , the nearest giant cluster ($cz = 1100\ km\ sec^{-1}$). The component of motion of the Local Group toward the Virgo cluster is $455 \pm 54\ km\ sec^{-1}$.

Studies of luminosities and redshifts of all-sky samples of field galaxies and clusters generally have yielded in-fall velocities toward Virgo in rough agreement with the measurement reported here. [See Davis *et. al.*, (1980) and Peebles (1978) and reference therein.] Velocities span a range from a recent measurement of $480 \pm 75\ km\ sec^{-1}$ (Aaronson *et.*al., (1980) to a null result of $\pm 25\ km\ sec^{-1}$ (Visvanathan and Sandage; 1977).

How did the Local Group acquire its velocity? If the Virgo cluster represents excess mass density which is stationary with respect to co-moving coordinates, then the $455\ km\ sec^{-1}$ velocity toward Virgo may have resulted from gravitational acceleration toward the cluster acting

over a Hubble time. From observational evidence de Vaucouleurs has claimed that the Local Group is a member of a larger disk-like supercluster of galaxies centered on Virgo, and the Virgo cluster's recessional velocity is reduced by 250 $km\ sec^{-1}$ relative to an all-sky sample of galaxies (de Vaucouleurs, 1958, 1972; de Vaucouleurs and Peters, 1968). From theoretical invesigations, White and Silk (1979) have shown that galaxies positioned on the periphery of a collapsing aspherical system can acquire velocities accounting for the motion of the Local Group within the plane of a disk-like supercluster.

It was pointed out by Sandage *et.*al., (1972) that the relation between density inhomogeneities (e.g., the Virgo- centric overdensity) to distortions of the Hubble flow (e.g., the in-fall velocity toward Virgo) could yield a value for q_0 (Silk, 1974; Peebles, 1976; Davis *et. al.*, 1980; Yahil *et. al.*, 1980; Tammann *et. al.*, 1979).

A study of the magnitude-redshift relation for galaxies external to the Virgo cluster in the redshift range cz of 1500-6500 $km\ sec^{-1}$ by Rubin *et. al.*, (1976a,b), have yielded a solar motion of 600 $km\ sec^{-1}$ relative to their selection of galaxies. The combination of their velocity with the microwave velocity yields a motion of 800 $km\ sec^{-1}$ for the Rubin, *et. al.*, (1976a,b) shell relative to the background radiation. The large velocity would indicate that distant shell of galaxies does not form a stationary frame with respect to the 3 K background. Their work has been disputed by Schecter (1972) who claims their analysis neglects correlation amongst their model parameters with a consequent underestimation of errors by a factor of three.

b) Interpretation of Higher Order Limits

The lack of quadrupole anisotropy allows us to place limits on processes of cosmological interest.

Rotation of the universe (a *prima facie* contradiction to Mach's Principle) could influence the formation of galaxies and would in general yield quadrupole anisotropy in the radiation background. The effect of a rotating universe or net vorticity has been investigated by several authors (Hawking,1969; Collins and Hawking,1973a; Ruzmaikina and Ruzmaikin,1969; King

and Ellis,1973; Sciama,1971; Batakis and Cohen,1975; Novello and Reboucas,1978). In a high density, spatially closed universe, the effect corresponds to the transverse Doppler shift in a flat space. Our result puts a limit on the vorticity of about $7\times10^{-14}(R-1)^{-1}$ radians year^{-1}, where R is the ratio of the scale size of the universe now to that when the radiation was last scattered. R must be between about 7 and 1500 depending upon how much ionized intergalactic medium is present in the universe. However, in a low density open universe the effect is more complicated and these observations only place a limit on the vorticity of about 2×10^{-15} radians year^{-1}. In the low density model the observed temperature of the radiation would have anisotropic components of the form $cot(\theta/2)\,cos(\phi)$, where θ is the angle between the direction of observation and the preferred direction. This relation is valid only for angles greater than a few minutes of arc. In open models most of the anisotropy peaks near the preferred direction, so only weak limits can be set for less than complete sky coverage.

A chaotic field of random gravity waves with wavelengths of a megaparsec and longer might exist with sufficient energy density to close the universe. Such a field of gravity waves would appear quasistatic to us but would cause a temperature variation by the photon redshift. We might at this time be immersed in one of these gravity waves and the strain it produces here would appear as a minute anisotropy in the Hubble expansion. However, such an anisotropy could appear as a measurable quadrupole distribution in the background radiation. Burke (1975) has calculated the effect of such a local gravity wave and finds

$$\frac{\Delta T}{T} = \frac{1}{2}(1-\cos\theta)\cos 2\phi\ (A_e - A_o) \tag{25}$$

where θ is the angle between the direction of propagation for the gravity wave and the direction of observation, ϕ is the gravity wave polarization orientation angle, and A_e and A_o are the strains at the emitter and the observer respectively. Because our beam width is very large (approximately 7 degrees) we average over the strain at the emitter and the anisotropy is just proportional to the local strain.

The energy density in a gravity wave is given by the following expression

$$\rho_{GW} = \frac{\pi}{4}\frac{c^2}{G}\frac{1}{\lambda^2}|A|^2. \tag{26}$$

If we combine the equations and evaluate numerically we find

$$\rho_{GW} = 0.9\,\rho_{critical}\left(\frac{6\ Mpc}{\lambda}\right)^2\left(\frac{\Delta T}{1\ mK}\right)^2 \tag{27}$$

where $\rho_{critical} \approx 2\times10^{-29}$ gm/cm^3 is thought to be the density necessary to close the universe. Thus our measurement indicates that gravity waves with wavelengths longer than about $\lambda = 6$ Mpc do not have an energy density sufficient to close the universe. These results are the most restrictive to date. Measurements of the polarization of the cosmic background radiation have produced limits somewhat higher than these for extremely long wavelength gravity waves (Caderni, *et. al.*, 1978; Lubin and Smoot, 1979; and Nanos, 1979) and can be thought of as independent tests since they are sensitive to distant gravity waves and not to any local one.

The limits on quadrupole anisotropy restrict the anisotropic shear expansion of the universe. Many authors (Rees,1968; Collins and Hawking,1973b; Doroshkevich, Lukash, and Novikov,1974) have calculated the effects on anisotropic expansion on the isotropy of the cosmic radiation. The results, though somewhat model dependent, depend most strongly upon the time of last scattering because all viable models tend toward isotropic expansion, as a result of the great isotropy of the radiation at present. The 1 mK limit on anisotropy corresponds to

$$\frac{\Delta H_0}{H_0} \approx 3\times10^{-4}\ R^{-3/2}. \tag{28}$$

Here again polarization measurements make a nearly independent and complementary measurement of this effect. Depending upon the density of intergalactic medium the polarization measurement is equally sensitive for relatively late last scatterings and only about 3% as sensitive for early last scatterings.

There are some arguments (Olson;1978) that the abundance of helium is a sensitive probe of the isotropy and homogeneity of the universe. In some simple models the abundance of helium sets a limit of 10^{-12} on $\Delta H_0/H_0$. However, Olson and Silk (1978) have presented models of anisotropic expansion that still yield observed helium abundances. The isotropy of the cosmic background remains the most direct probe of the global isotropy of the universe.

If causality holds and the homogeneity and anisotropy of the universe is achieved by physical transport of energy and matter, then we should expect that parts of the universe separated by distances much larger than their event horizon at the epoch of last scattering will be inhomogeneous. Therefore, the cosmic background radiation ought to exhibit anisotropies ("sky roughness") for angular scales greater than about 3^{o} to 75^{o} depending upon whether the last scattering occurred at a redshift of 1500 or 7 respectively (Weinberg; 1972, p.525). We see no evidence for such anisotropy.

VI. CONCLUSION

The principal result of this work is the detection of dipole anisotropy in the 3 K cosmic background radiation. The magnitude of the anisotropy is $3.61 \pm 0.54\, mK$, one part in 800 of 3 K, in a direction not accounted for by the velocity of the sun about the Galaxy or relative to the Local Group. The inferred motion of the sun relative to the 3 K radiation is $361 \pm 54\, km\ sec^{-1}$, toward 11.23 ± 0.46 hours R.A., $19.0 \pm 7.5^{\circ}$ declination.

The limits the data places on most components of quadrupole anisotropy are about one part in 3000 of 3 K, or less than one part in three of the amplitude of dipole anisotropy. The limits the data places on "sky-roughness" on a 7° angular scale is about one part in 6000 of 3 K, less than one part in six of the dipole amplitude. The dipole anisotropy identifies the local co-moving frame with respect to which the dynamics of the neighboring galaxies should be best understood. However, the "discovery" of the local frame of rest may exacerbate the already existing conflicts in the determination of the local velocity field of galaxies. The lack of additional anisotropy re-emphasizes the theoretical problem of accounting for the extreme isotropy of the radiation.

Two important extensions of this work are in progress. Observations in the southern hemisphere are a crucial check of the global nature of dipole anisotropy, and provide independent measurement of the quadrupole parameters. Four flights from Lima, Peru (12° South Latitude) have taken place and the initial results have been reported (Smoot and Lubin, 1979). Secondly, a next generation experiment is being designed as part of a proposed satellite, the **C**osmic **B**ackground **E**xplorer (**COBE**). The plan is for a year long survey of the entire celestial sphere at four microwave frequencies. With increased sensitivity afforded by the long exposure and improvements in receiver design, it will be possible to search for higher moments of anisotropy with a sensitivity of about one part in 30 of the $3.6\, mK$ dipole amplitude.

ACKNOWLEDGEMENTS

This work was supported by the National Aeronautics and Space Administration and by the High Energy Physics Research Division of the U.S. Department of Energy under contract No. W-7405-ENG-48.

We acknowledge the important contribution made by R.A. Muller and J.A. Tyson during the inital phase of this work.

We very much value the contributions made by the members of the Earth Survey Aircraft facility at NASA-Ames, including J. Cherbonneaux, M. Knutson, J. Barnes, R. Erikson, C. Webster, R. Williams and J. Wahl. These flights would not have been possible without the support of N. Boggess of the National Aeronautics and Space Administration and R. Birge and A. Sessler of the Lawrence Berkeley Laboraory.

We thank C. Witebsky for his assistance with estimates of the galactic background, S. Friedman, S. Peterson, P. Lubin, and other members of our group for their support, help, and encouragement. This work would not have been possible without the diligent efforts of our staff J.S. Aymong, H. Dougherty, J. Gibson, N. Gusack, M. McBride, and J. Yamada.

REFERENCES

Aaronson, M. Mould, J., Huchra, J. Sullivan, W., Schommer, R., and Bothun, G. 1980, *Ap. J.* in press.

Batakis, N., and Cohen, J.M. 1975, *Phys. Rev.*, **D12,** 1544.

Birkinshaw, M., Gull, S.F., and Northover, K.J.E. 1978, *M.N.R.A.S.*, **185,** 245.

Boughn, S.P., Fram, D.A., and Partridge, R.B. 1971, *Ap. J.*, **165,** 439.

Burke, W.L. 1975, Ap. J., **196,** 329.

Caderni, N., Fabbi, R., Melchiorri, B., Melchiorri, F., and Natale, V. 1978, *Phys. Rev.*, **D17,** 1901.

Cheng, E.S., Saulson, P.R., Wilkinson, D.T., and Corey, B.E. 1979, *Ap. J. Lett.*, **232,** L139.

Collins, C.B., and Hawking, S.W. 1973a, *M.N.R.A.S.* **162,** 307.

Collins, C.B., and Hawking, S.W. 1973b, *Ap. J.*, **180,** 317.

Compton, A.H., and Getting, I.A. 1935, *Phys. Rev.*, **49,** 817.

Conklin, E.K., and Bracewell, R.N., 1967, *Nature* **216,** 777.

Conklin, E.K. 1969, *Nature* **222,** 971.

Corey, B.E. 1978, *Ph. D. Thesis* Princeton University.

Corey, B. E. 1979, private communication.

Corey, B.E. and Wilkinson, D.T. 1976, *Bull. Astron. Astrophy. Soc.* **8**, 351.

Davis, M., Tonry, J., Huchra, J., and Latham, D. W. 1980, *Ap. J.* Submitted.

de Vaucouleurs, G. 1958, *Nature* **182,** 1478.

de Vaucouleurs, G. 1972, *IAU Symposium No. 44,* (Reidel, New York, p. 353).

de Vaucouleurs, G. and Peters, W.L. 1968, *Nature* **220,** 868.

de Vaucouleurs, G., de Vaucouleurs, A. Coravin, H.G., 1976, *Second Reference Catalogue of Bright Galaxies* (University of Texas, Austin).

Dicke, R.H., Peebles, P.J.E., Roll, P.G. and Wilkinson, D.T. 1965, *Ap. J.* **142,** 414.

Doroshkevich, A.G., Lukash, V.N., and Novikov, J.D. 1974, *Sov. Astron.* Vol. **18,** No. 5.

Gorenstein, M.V., Muller, R.A., Smoot, G.F. and Tyson, J.A. 1978, *Rev. Sci. Instrum.* **49,** 440.

Hagfors, T. 1970, *Radio Sci.* **5,** 189.

Hawking, S. 1969, *The Observatory* **89,** 38.

Henry, P.S. 1971, *Nature* **231,** 516.

Hirabayashi, H. 1974, *Publ. Astron. Soc. Japan* **26,** 263.

Janssen, M.A., Bednarczyk, S.M., Gulkis, S., Marlin, H.W., and Smoot, G.F. 1979, *IEEE Trans. Antennas Propagat.,* Vol. **AP-27,** No. 4.

King, A.R., and Ellis, G.F.R. 1973, *Comm. Math. Phys.,* **31,** 209.

Kraus, J.D. 1966, *Radio Astronomy,* (McGraw-Hill, New York).

Lang, K.R 1974, *Astrophysical Formulae* (Springer-Verlag, New York).

Linsky, J.L. 1973, *Ap. J. Supplement Series No. 216* **25,** 163.

Lubin, P.M., and Smoot, G.F. 1979, *Phys. Rev. Lett.* **42,** 129.

Martin, B.R. 1971, *Statistics for Physicists,* (Academic Press).

Mayer, C.H. 1970, *Surfaces and Interiors of Planets and Satellites,* edited by A. Dollfus, (Academic, New York), p. 180.

Muehlner, D.J. and Weiss, R. 1976, *Infrared and Submillimeter Astronomy,* Astrophysics and Space Sciences Library, (Reidel, Hingham, MA), Vol. **63.**

Nanos, G.P. 1979, *Ap.J.,* **232,** 341

Novello, M., and Reboucas, M.J. 1978, *Ap.J.,* **225,** 719.

Olson, D.W. 1978, *Ap.J.,* **219,** 777.

Olson, D.W., and Silk, J. 1978, *Ap.J.,* **226,** 50.

Partridge, R.B. and Wilkinson, D.T. 1979, *Phys. Rev. Lett.* **18,** 557.

Peebles, P.J.E. 1971, *Physical Cosmology* (Princeton U.P., Princeton, N.J.).

Peebles, P.J.E. 1976, *Ap.J.* **205,** 318.

Peebles, P.J.E. 1978, *Comments on Astrophysics* **VII,** 197.

Peebles, P.J.E. and Wilkinson, D.T. 1968, *Phys. Rev.* **174,** 2168.

Penzias, A. A. and Wilson, R. W. 1965, *Ap. J.* **142,** 419.

Penzias, A. A. and Wilson R. W. 1966, *Ap. J.* **146,** 666.

Rees, M. J. 1968, *Ap.J.*, **153,** L117.

Rubin, V.C., Ford Jr., W.K., Thonnard, N., Roberts, M.S., and Graham, J. A. 1976a, *Astro. J.*, **81,** 687.

Rubin, V.C., Thonnard, N., Ford Jr., W.K., and Roberts, M.S. 1976b, *Astro. J.* **81,** 719.

Ruzmaikina, T.V. and Ruzmaikin, A.A. 1969, *Soviet Physics JETP* **29,** *5, 934.*

Sandage, A., Tammann, G.A., and Hardy, E. 1972, Ap.J. **172,** 253.

Schechter, P.L. 1977, *Astron. J.* **82,** 569.

Schmidt, M. 1965, in *Stars and Stellar Systems, Vol. IX Galactic Structure,* (University of Chicago Press, 513).

Schwartz, D.A. 1970, *Ap.J.* **162,** 439.

Sciama, 1971, *Modern Cosmology,* Cambridge University Press.

Silk, J. 1974, *Ap.J.* 193, 525.

Smoot, G.F., Gorenstein, M.V. and Muller, R.A. 1977, *Phys. Rev. Lett.* **39,** 898.

Smoot, G.F., and Lubin, P.M. 1979, *Ap.J.* **234,** L117.

Staelin, D.H., Kunzi, K.F., Pettyjohn, R.L, Poon, R.K.L., Wilcox, R.W., Waters, J.W. 1976, *J. of Appl. Meteor.*, **15,** 1204.

Tammann, G.A., Yahil, A., and Sandage, A. 1979, *Ap. J.* **234,** 775.

Taylor, R.E. 1973, *Proc. IEEE* **61,** 469.

Visvanathan, N. and Sandage, A. 1977, *Ap.J.*, **216,** 214.

Webster, A.S. 1974, *M.N.R.A.S.* **166,** 355.

Weinberg, S. 1972, *Gravitation and Cosmology: Principles and Applications of the General Theory of Relativity* (John Wiley & Sons, New York).

White, S.D.M., and Silk, J. 1979, *Ap. J.* **231,** 1.

Woody, D.P., and Richards, P.L. 1979, *Phys. Rev. Lett.* **42,** 925.

Yahil, A., Tammann, G.A. and Sandage, A. 1977, *Ap. J.* **217,** 903.

Yahil, A. Sandage, A., and Tammann, G.A. 1980, *Physica Scripta* **21,** 635.

APPENDIX A - RADIOMETER CALIBRATION

The 33 GHz receiver gain is sufficiently stable such that a single calibration constant converts the anisotropy measured in empirical units to milli-Kelvins. Multiple measurements performed in flight establish that the radiometer gain is constant to $\pm$ 2%. Ground-based calibrations, confirmed in flight, provide an absolute calibration with an rms uncertainty of 4%. The uncertainty in the radiometer calibration is a small part of the error budget and degrades the signal-to-noise ratio of the cosine anisotropy by a negligible 1%.

a) Stability of the Radiometer Gain and Noise Temperature

Three in-flight indicators monitor the stability of the system noise temperature and the gain of the 33 GHz radiometer. At altitude the total noise temperature of the radiometer, nominally 600°K, is dominated by the noise generated in the mixer. External contributions to the noise temperature are minimal: the cosmic background adds 3 K, and the atmospheric signal adds only 60 mK. The noise monitor measures the detected I.F. power level, a signal proportional to the product of the noise power in the radiometer, and the system gain up-stream of the detector diode. In a typical flight, the noise-monitor signal drops 2% during the initial cool-down leg, then drifts downward an additional 2% during the remainder of the flight. The rms variation between the mean noise monitor signals for the various flights is $\pm$ 0.4%.

A second indication of relative system gain is the magnitude of the rms fluctuations of the 33 GHz data words recorded every two seconds. The rms fluctuations are proportional to the system noise temperature. The data analysis programs compute the rms fluctuations for some 5000 edited data words recorded in a typical flight. Data from each flight yield a measurement of rms fluctuations that varies among flights by $\pm$ 0.75%. Receiver noise alone accounts for this variation: with 5000 words recorded in a flight, we expect the rms fluctuations to be measured with an error of $\pm\sqrt{5000}/2 = \pm 0.0071$, or 0.71%.

Finally, aircraft banks inject a 24 mK signal into the 33 GHz radiometer and provide a final indication of system gain. In a typical flight, the U-2 changes headings between data legs

by banking at a nominal roll angle of 21°. During a bank the antennas receive unbalanced contributions of atmospheric thermal radiation yielding the 24 mK signal. The atmospheric thermal radiation provides a test signal which we use to compare the system gain between flights. Receiver noise and uncertainty in sidelobe illumination by the earth yield a net uncertainty of $\pm 2.4\,mK$, or $\pm 10\%$ of the total signal. Within these errors, the banking data are consistent with the hypothesis of constant system gain.

Although we would prefer independent measurements of both receiver gain and system sensitivity to $\pm 2\%$ or better, we feel that the various monitors described here, taken together, justify using a single calibration constant. The error in this conversion constant is then limited by the uncertainty of the absolute receiver calibration.

b) Absolute Radiometer Calibration

The statistical errors in estimates of cosine anisotropy are about 10%. It is necessary to obtain an absolute calibration whose uncertainty minimally degrades the sensitivity of the measurement. We feel the procedures described below determine the absolute radiometer calibration to $\pm 3\%$.

Blackbody targets of Eccosorb AN 72 placed over the mouths of the horn antennas calibrate the 33 GHz radiometer in the laboratory. Eccosorb AN 72 is a commercial microwave absorber made of urethane foam impregnated with graphite. The radiometer is calibrated by covering one horn mouth with a room-temperature target at $300\,K$ and the other with a target soaked in liquid nitrogen (LN) at $77\,K$. These fill both antenna beam patterns with uniform temperature blackbodies and establish a nominal $223\,K$ signal difference between the arms of the radiometer. The AN 72 is porous: a target withdrawn from a bath of LN maintains a stable temperature to within a degree Kelvin for more than 30 seconds while the LN boils off. The measured difference in signal strength between a target immersed in LN and one withdrawn from a bath is less than a degree Kelvin. The digitized signal difference is recorded and yields the desired calibration. Several repetitions of the procedure, with the loads interchanged over the antenna mouths, check the consistency of the measurements.

The empirical rms variation between these calibrations over a several month period is $\pm 2.1\%$. The contribution of receiver noise to this error is negligible, and the uncertainty in physical temperature difference between the two loads for any one measurement is about $\pm 0.5\%$. The probable origin of the 2% fluctuation is a combination of receiver temperature variation between the calibrations and variations in the exact way the cold target is held over the antenna mouths. If the cold target is held exactly perpendicular to the antenna beam axis, then dielectric reflection from the LN decreases the signal difference between the calibrators. We measured this reflection to be about 1% and found that tilting the surface of the cold Eccosorb about 10° from the beam axis reduces the reflection below 0.1%.

We correct for the saturation of the detector diode during the LN calibration procedure. Two different operating points of the diode are used for the room-temperature versus LN calibration. Ideally the detector diode (an HP 8472B negative) is a square law device whose voltage output is proportional to the IF input power. However, putting various attenuators before the detector diode to measure the diode response shows that the target signal of 290 K slightly saturates the diode, reducing the system gain by 5% compared to the case when both antennas see cold signals.

The moon calibrations, performed in-flight, cross-check the ground-based measurements: each receiver configuration has been calibrated at least once by pointing an antenna at the moon during a flight. The calibration constant determined from moon observations is within 5.4% of the ground-based results, consistent with the 6% uncertainty in the moon calibration.

The moon fills a small fraction of the solid angle subtended by the antenna beam. Thus, the antenna temperature of the moon, $T_{antenna}$, is given by

$$T_{antenna} = T_{lunar\ disk} \frac{\Omega_{moon}}{\Omega_{antenna}} \qquad (A.1)$$

where

$T_{lunar\ disk}$ = the mean antenna temperature of the lunar disk used to calibrate the radiometer.

Ω_{moon} = the solid angle subtended by the moon. The mean solid angle is 0.211 square degrees, and varies by ± 15% during the lunar orbit. The apparent diameter of the moon is tabulated in the American Ephemeris and Nautical Almanac with an error that is negligible for our purposes.

$\Omega_{antenna}$ = the antenna beam width which spans a solid angle of 69.3 ± 0.7 square degrees.

The temperature of the lunar disk is the main uncertainty in this calibration procedure. The radiation temperature at the center of the lunar disk has been measured at centimeter wavelengths (Hagfors, 1970; Mayer, 1970; Linsky, 1973) to be

$$T_{lunar\ center} = (215 \pm 4)K + (34 \pm 3)\cos(\phi - 41^\circ \pm 3^\circ)K \qquad (A.2)$$

where

ϕ = the phase of the moon after the full moon.

Our measurement includes the whole lunar disk. This has the advantage that variations in antenna temperature due to the lunar phase are reduced, but adds additional uncertainty in the estimate of temperature and emissivity variations over the lunar disk. According to Hagfors (1970), the emissivity at the center of the lunar disk is 0.97 due to dielectric reflection. Greater reflection near the edges reduces the net thermal signal by an additional 6% compared to the center. The result is

$$T_{lunar\ disk} = (202 \pm 7.5)K + (27^{+5.1}_{-2.5})\cos(\phi - 41^\circ \pm 3^\circ)K. \qquad (A.3)$$

A final correction to the lunar antenna temperature is due to navigational errors that misdirect the antenna slightly during a moon run. The pilots check the altitude of the moon during the run, and the resulting corrections are at most one-half degree, with less than a percent error increase in the final calibration constant.

APPENDIX B - SYSTEMATIC ERRORS AND CORRECTIONS

There are a significant number of systematic errors which could affect the anisotropy measurements. However, the corrections are small compared to the anisotropy signal and the residual systematic errors are appreciably smaller than the statistical errors.

a) Astrophysical Backgrounds and Corresponding Corrections

The decreasing flux of Galactic synchrotron and HII emission toward high frequencies motivated the choice of the 33 GHz observation frequency. However, there is a barely significant flux remaining at centimeter wavelengths that requires small corrections to the data. We have also estimated the effect of emission from galactic dust and found it neligible. Figure 5 illustrates the frequency dependence of antenna temperature for galactic synchrotron, HII, and dust emission.

i) Galactic Synchrotron Radiation

The primary source of extraneous background emission in this experiment is caused by relativistic electrons spiraling in the weak magnetic field of our Galaxy. This "synchrotron" radiation is highly anisotropic: the radiation is most intense towards the galactic center and is about a factor of 10 lower towards the anti-center and the galactic poles.

The corrections to the 33 GHz data are primarily based on a map of galactic synchrotron emission at 400 MHz compiled by R.E. Taylor (1973). A single scale factor extrapolates the emission to the antenna temperature at 33 GHz:

$$T_{33\,GHz} = T_{0.4\,GHz}\left[\left(\frac{33\,GHz}{8\,GHz}\right)^{-2.9}\left(\frac{8\,GHz}{0.4\,GHz}\right)^{-2.8}\right] \qquad \text{(B.1)}$$

The two spectral indices account for the apparent steepening of synchrotron emission above 8

GHz (Hirabayashi, 1974; Webster,1974; Penzias and Wilson, 1966; and Conklin, 1969). These data, folded with the antenna beam pattern, correct the measurements for each flight path. Figure 4 is a three dimensional projection of the sum of the contributions of diffuse galactic synchrotron emission with point-like HII sources along the galactic plane.

ii) HII Regions

The second major source of galactic radio interference is thermal emission from clouds of ionized hydrogen gas heated by the ultra-violet radiation of nearby stars. The Orion nebula is one classic example. Figure 5 shows the antenna temperature spectrum of a typical HII region. Unlike synchrotron emission, which is diffuse throughout the celestial sphere, most HII regions are confined to within 2° of the galactic plane, and appear as point sources in Figure 4. We compiled a list of HII regions from the Parkes survey as well as a number of other studies. The more important of these sources can be found in a general compilation by Lang (Lang, 1974, pg. 121-127; Kraus, 1966, pg. 246-248). Our sky coverage avoids most of these sources, and the contamination of the data by HII emission is slight: two measurements in the data required corrections of 0.1 and 0.2 *mK*, respectively, with errors of ±15%. All other corrections were less than 0.05 *mK*.

b) Corrections for Aircraft Roll

We monitored the atmospheric emission with the 54 GHz radiometer. The most significant source of atmospheric background resulted from non-level flight; however the aircraft roll generated an almost negligible background for the anisotropy measurement. The U-2 roll-attitude is quite stable: deviations from the mean roll for a flight path were typically less than 0.3°, requiring corrections to the measurements of no more than 0.4 mK.

A series of aircraft banks from 5° to 25°, performed over several flights, determined the ratio of atmospheric imbalance signal to bank angle,

$$\frac{\Delta T_{33\ GHz}}{^{\circ}\text{roll}} = 1.22 \pm 0.12\ mK/^{\circ}roll \qquad \text{(B.2)}$$

$$\frac{\Delta T_{54\ GHz}}{^{\circ}\text{roll}} = 220 \pm 10 mK/^{\circ}\text{roll}. \qquad \text{(B.3)}$$

Since the rms receiver sensitivity at 54 GHz is $100\,mK/\sqrt{\text{Hz}}$, an integration for two seconds measures a roll to an accuracy of $\pm 0.32^{\circ}$ in angle. This in turn corresponds to a measurement of atmospheric imbalance at 33 GHz with an error of $\pm 0.4\,mK$.

The correction to the 33 GHz signal for roll is straight-forward. The mean roll signal, $\Delta T_{54\,GHz}$, is computed for each flight path in a manner which is exactly analogous to the computation of the mean 33 GHz anisotropy signal. The correction to the 33 GHz signal is then proportional to the deviation of the 54 GHz signal from its mean value.

c) Antenna Sidelobes

The antennas have extremely low sidelobes; however, both the earth and aircraft are strong emitters and cover large solid angles. We estimate that the combined total power received by each antenna from the earth and aircraft was no more than 4 mK, and that the differential power received by the two antennas did not exceed 0.2 mK based on measured variations in the emissivity of the earth (Staelin, *et.al*; 1976).

Since most of the data were taken near the coast with the Pacific Ocean on one side and the Sierra Madre Range on the other, we wanted a cross-check on the estimated sidelobe rejection. A first check came from flying identical flight plans at different sidereal time and observing that the anisotropy changed signs as it should when the observed portion of the sky changed. The anisotropy changed its sign back when we reobserved the original sky position. Signals correlated with geographical features would not yield this signature of sign reversals. The second check came from data taken during aircraft banks where one antenna received more of the earth's radiation than the other. By matching two banks in opposite directions, one can more accurately determine the differential emission from the earth.

These procedures have allowed us to place a 0.5 mK limit on the possible anisotropic radiation from the earth during level flight. We estimate the effect of anisotropic earth shine on the cosine anisotropy by assuming a 0.2 mK signal correlated with geographical features (increased emissivity from landward directions for example). Incorporating such errors in fits

to the data yields a systematic contribution of 0.1 mK to the cosine parameters. As mentioned in section IV *(a)*, we increase our errors by 25% to take this contamination into account.

d) Horn Antenna Temperature Differential

The 33 GHz horn antennas were designed to have a low insertion loss to reduce spurious unbalanced thermal emission. With a measured insertion loss of 1.5%, each antenna at a physical temperature of 300 K radiates a 4.5 K signal into the receiver. Physical temperture differences of $300\,mK$ would then contribute a 4.5 mK anisotropy signal. In principle, the periodic interchange of the horn antennas would cancel this signal, in the same way in which the 60 mK offset of the ferrite switch is cancelled by the horn interchange. However, the physical temperature of the antennas can oscillate in synchrony with the antenna rotation: the exchange of the antennas every 64 seconds exposes them to variations in the airstream between opposite sides of the aircraft.

This problem is exacerbated by the large temperture gradient down the antenna bodies. The antennas are purposely exposed to avoid the additional signal that would be produced by a window. Thus they are exposed to the cold, $-40^{\circ}C$, slipstream, and serve the dual purpose of acting as "cooling fins" which extract heat from the aluminum thermal ballast. (The ballast in turn acts as the heat sink for the radiometer electronics maintained at about $26^{\circ}C$). The result is that the large ends of the antennas, just barely in the slipstream, cool to $-35^{\circ}C$, while the small ends buried in the aluminum block are maintained at $26^{\circ}C$.

The insertion loss per unit length varies inversely with the cross-sectional diameter of the horn aperature, so it is the small ends of the horn antennas that contribute the major portion of the thermal re-emission. Fortunately, they are farthest from the wind, and moreover are thermally shorted by the aluminum ballast. Two pairs of sensors monitor the temperature differences between the mouths and mid-points of the horn antennas through the flight. The data acquisition system records these differences once every four seconds.

The data show that the difference profile does oscillate in synchrony with the alternation

of the antenna orientation. The amplitude of this oscillation, measured by the mid-point sensors, is typically 100 mK (physical temperature), and is remarkably stable. The amplitude varies less than 5% during a flight from rotation to rotation independent of aircraft heading.

The periodic reversal of the aircraft heading can reveal spurious radiometric signals that oscillate in synchrony with the antenna rotation. As discussed in subsection, *(f)*, such a "rotation-offset" signal is in fact detected as $2 \pm 0.5\ mK$ and appears stable, within statistics, throughout a flight. An oscillating 100 mK thermal difference signal combined with a few percent insertion loss may contribute some or all of this rotation offset. The stability of the amplitude of the thermal difference oscillation to 5% gives us confidence that the interchange of the aircraft flight path cancels the unknown contribution of the thermal oscillation to the rotation offset to less than 2 mK times 0.05, or 0.1 mK.

e) The Motion of the Earth about the Sun

The 30 $km\ sec^{-1}$ motion of the earth about the sun produces an anisotropy of $0.3 \pm 0.03\ mK$ magnitude; the 10% uncertainty is in the measured temperature of the $3\ K$ background radiation. The $0.3\ mK$ signal is not a correction in the usual sense, but must be removed from the data to compute the anisotropy in a barycentric coordinate system. The value subtracted from each measurement is proportional to the component of the earth's motion along the difference vector of the antenna directions:

$$\Delta T_{33GHz} = 3\,\mathrm{K} \cdot \frac{\vec{v}_{earth}}{3.0\times10^{5}\,\mathrm{km}\,sec^{-1}} \cdot (\hat{n}_1 - \hat{n}_2) \qquad \text{(B.4)}$$

where

$\hat{n}_1$, $\hat{n}_2$ are the direction vectors of antenna 1 and 2 for the measurement

$\vec{v}_{earth}$ is the velocity of the earth about the sun for the epoch of the measurement.

The uncertainty of this correction is negligible compared to the statistical uncertainty in the measure of anisotropy parameters.

f) The Rotation Offset

Plots of the 33 GHz data, signal-averaged at the rotation period, show a change in signal level between the two antenna orientations which is independent of aircraft heading. There is no evidence for a slope or spurious fluctuations during a rotation cycle, and this "rotation offset" appears constant throughout a flight. Thus the mean difference between anisotropy measured in sequential pairs of flight paths represents the celestial anisotropy, while the mean sum is the rotation offset. The offset is measured in a given flight with an uncertainty of $\pm 0.5\ mK$, and its value for each flight is plotted in Figure 6.

The rotation offset is of some concern because its origin is uncertain. The data in Figure 6 suggest that a major component of the effect is internal to the apparatus, simply because the rotation offset changed appreciably as the equipment was being modified during the early flights. However, care was taken to minimize or eliminate electrical interaction between the rotation system and the 33 GHz radiometer. The rotation electronics are isolated from the 33 GHz radiometer by employing separate grounds and power feeds. Resistors isolate the monitoring limit-switches from the data recording system, and a mechanical relay shuts off the power to the rotation system during periods of data taking. After flight 12, a five hour ground test attempted to measure the offset. Care was taken to insure equal signals in each antenna, however the test gave an inconclusive result of $1.1 \pm 0.5\ mK$.

Two other possible origins for the rotation offset are asymmetric radiation into the antenna sidelobes from the aircraft wings and asymmetric cooling of the antennas by the airstream. A pair of temperature sensors, one at each antenna mid-point, measured the temperature difference in flight. The sensors were placed along a flange 4 cm from the horn surface to avoid drilling into the horn body; therefore, it is difficult to extrapolate the temperature variations within the 1 micron skin depth at the surface. However, the sensor signals did have one striking property in common: in all flights, the signal showed clear triangular or quasi-sinusoidal oscillations synchronized with the rotation period. This is evidence that the mid-point temperatures are in fact driven up and down by the wind as the antennas rotate. Moreover, the

amplitude and shape of the signal was stable throughout a given flight. The amplitude of the effect is small, however, ranging from 40 to 100 mK between the different flights. In addition, flight 12, where the temperature difference was the highest (100 mK), produced the smallest rotation offset ($\simeq$ 0.3 mK).

Although the behavior of the temperature sensor signals does not correlate well with the behavior of the rotation offset, we can use the magnitude of the rotation offset to place a limit on the size of the spurious anisotropy that results from variations in the physical temperature of the antennas. The amplitude of the mid-point temperature sensor oscillation is stable to about 10% within a single flight. Residual differences in the spurious signal between leg-measurements should be at most 10% of 2 mK or 0.2 mK. In addition, the amplitude of oscillation varies smoothly between measurements, so that differences cancel even below 0.2 mK.

The residual differences between pairs of measurements are uncorrelated with the antenna direction in the sky. The origin of the rotation offset is unknown; however, since it appears constant and stable throughout a flight, we believe that it is substantially canceled as the aircraft heading is periodically reversed, and the effect on the parameters of cosine anisotropy is negligible compared to the statistical errors.

M.V. Gorenstein, Bldg. 54 Room 418, MIT, Cambridge, MA 02139 G.F. Smoot, Bldg. 50 Room 230, Lawrence Berkeley Laboratory, Berkeley, CA 94720

TABLE 1

Flight Circumstances

Flight	Date Launch-Land (UT)	Exposure[a] (hours)	Receiver[b] Sensitivity (mK/Hz$^{1/2}$)	Configuration and Performance
			Engineering Flights	
1	7 July 76 1705-1924	---	Paramp	Daylight flight. Paramp overheated.
2	6 Aug 76 1800-2044	---	Paramp	Daylight flight. Systems work nominally.
3	23 Sept 76 0100-0620	---	Paramp	Nighttime flight. Rotation system and digital recorder fail at altitude due to cold.
			Data Flights with Equipment in Preliminary Configuration	
4	3 Dec 76 0132-0541	2.78	Paramp 96 ± 9	Regrease rotation bearing, rebuild temperature sensitive electronics. Paramp noise high, gain changes with temperature. Include moon calibration.
5	10 Dec 76 0225-0623	2.83	Paramp 119 ± 19	Reduce interchange period of antennas from once/128 seconds, to once/64 seconds. Similar performance as in flight 4.
6	2 Feb 77 0130-0615	3.83	"old" mixer 119 ± 1	Replace paramp with mixer, and install resistive heaters in ballast. Receiver gain drift is less than 0.04 db/hour. Receiver noise 30% high. Include upon calibration.

7	18 Mar 77 0220-0702	3.85	"old" mixer 96 ± 1	Include 180° phase switch on this and subsequent flights. Install heater in digital recorder. System operates nominally.
			Data Flights with Equipment in Finalized Configuration	
8	1 Apr 77 0200-0608	3.23	"new" mixer 44.1 ± 0.3	Install new mixer-based receiver, shield ferrite switch with mu-metal, set 180° phase-switch period to 24 seconds. Receiver sensitivity comparable to pre-flight measurements. Ferrite switch offset stable at 30mK. Equipment configuration unchanged in succeeding flights.
9	14 Apr 77 0600-1041	3.55	"new" mixer 43.8 ± 0.3	Nominal equipment operation.
10	20 Apr 77 0112-0450	3.87	"new" mixer 44.1 ± 0.3	Nominal equipment operation.
11	27 May 77 0300-0744	3.52	"new" mixer 43.8 ± 0.3	Nominal equipment operation. Publish results of flights 4-11 (Smoot, et. al. 1977).
12	8 Sept 77 0230-0705	3.57	"new" mixer 44.0 ± 0.3	Radiometer-arm-offset 130mK.
13	24 Feb 78 0130-0615	3.61	"new" mixer 44.3 ± 0.3	Open radiometer enclosure for first time since 8th flight and null ferrite switch offset. Nominal equipment operation.
14	16 May 78 0241-0745	3.54	"new" mixer 44.8 ± 0.3	Null ferrite switch offset. Include moon calibration. Nominal equipment operation.

[a]Interval during which anisotropy data was collected at altitude. Time includes periods of banks, antenna rotations, and calibrations.

[b]Receivers used:

Paramp - room-temperature 33.5 GHz degenerate parametric amplifier. Noise temperature measured on ground was 250K, with 300 MHz i.f. bandwidth, however, system temperature increased in flight and thermal gain coefficient was unacceptibly large, -0.4db/C.

"old" mixer - room-temperature 33.0 GHz mixer-based receiver. System temperature (double-sideband) was about 1,000K with 500 MHz i.f. bandwidth.

"new" mixer - room-temperature 33.0 GHz mixer-based receiver. System temperature (double-sideband) was about 630K on ground and in flight with 1,000 MHz i.f. bandwidth.

TABLE 2

Measurements of Anisotropy in 3 Kelvin Radiation: Flights 4-14

Flight	Path	Time	$\Delta T_{3K} \pm \sigma$	$\hat{n}_R$		$\hat{n}_L$		$\Delta\chi^2$
				R.A.	Dec.	R.A.	Dec.	
		(UT)	(mK)	(hr.)	(°)	(hr.)	(°)	
(1)	(2)	(3)	(4)	(6)	(7)	(8)	(9)	(10)
4	1	2:28	-4.5 ± 2.7	22.2	+11	1.4	+59	
	2	2:50	5.6 2.8	1.7	59	22.3	11	
	3	3:13	-1.2 2.9	23.0	11	2.1	59	
	4	3:36	0.1 2.8	2.5	59	23.4	11	
	6	4:21	3.2 2.4	3.5	32	22.6	32	
	7	4:52	-4.5 2.9	23.2	32	4.0	32	
5	1	3:03	-1.0 ± 3.1	23.3	+11	2.4	+59	
	2	3:24	4.1 3.6	2.8	59	23.6	11	
	3	3:48	-2.0 4.9	0.3	9	2.8	63	
	4	4:11	-4.6 3.6	3.0	63	0.8	8	
	6	4:57	3.2 2.7	4.5	33	23.7	33	
	7	5:30	-1.9 2.9	0.3	32	5.1	32	
6	3	2:43	5.8 ± 3.7	4.7	+12	1.2	+57	
	4	3:05	-6.2 3.7	1.6	57	5.1	12	
	5	3:26	-0.2 3.6	5.4	12	2.0	57	
	6	3:48	-5.0 4.0	2.3	57	5.8	12	
	7	4:10	1.4 3.5	7.4	48	3.0	19	
	8	4:32	2.2 3.9	3.7	17	7.8	52	
	12	5:10	10.7 3.7	4.3	15	8.4	49	
	13	5:33	-10.3 3.9	8.8	49	4.7	15	
7	1	2:47	-2.6 ± 2.9	6.5	+ 7	6.5	+67	
	2	3:13	-2.6 2.8	6.9	67	6.9	7	
	3	3:37	-0.7 2.7	7.3	7	7.3	67	
	4	4:00	1.3 2.9	7.7	67	7.7	7	
	5	4:24	8.4 3.0	8.1	7	8.1	67	
	6	4:47	-0.1 2.9	8.5	67	8.5	7	
	7	5:08	2.9 2.8	11.1	33	6.3	31	
	8	5:32	-3.1 2.9	6.7	33	11.5	31	
	9	5:55	0.7 2.9	11.9	33	7.1	31	
	10	6:18	-3.1 2.7	7.5	33	12.3	31	
8	1	2:33	1.4 ± 1.3	7.1	+ 7	7.1	+67	1.3
	2	2:55	-2.3 1.6	7.5	67	7.5	7	1.8
	3	3:14	0.3 1.6	7.9	7	7.9	67	.0
	4	3:31	-0.6 1.5	8.1	67	8.1	7	.0
	5	3:48	2.6 1.6	10.8	32	5.9	32	.0
	6	4:06	-2.8 1.6	6.3	32	11.1	32	.2
	7	4:23	-0.5 1.7	11.3	32	6.5	32	2.2
	8	4:42	-1.9 1.6	6.9	32	11.7	32	.0
	9	5:01	4.3 1.6	12.0	32	7.2	32	3.2
	10	5:18	-1.1 1.6	7.5	32	12.3	32	.0

9	1	6:39	2.6 ± 1.6	12.1	+ 7	12.1	+67	.9
	2	6:58	-2.2 ± 1.6	12.4	67	12.4	7	.6
	3	7:16	1.1 ± 1.6	12.7	7	12.7	67	.0
	4	7:34	0.6 ± 1.5	12.7	67	13.1	7	.8
	5	7:52	-0.4 ± 1.4	13.3	7	13.3	67	.8
	6	8:09	-1.4 ± 1.4	13.3	67	13.7	7	.3
	7	8:26	-2.1 ± 1.5	16.2	31	11.4	32	.0
	8	8:45	3.3 ± 1.6	11.7	32	16.5	31	.3
	9	9:02	-2.3 ± 1.6	16.8	32	12.0	32	.0
	10	9:20	1.2 ± 1.5	12.3	32	17.1	32	1.0
	11	9:40	-4.3 ± 1.6	17.5	32	12.6	32	.8
	12	9:56	4.8 ± 1.6	12.9	32	17.7	32	1.2
10	7	3:16	1.8 ± 1.6	11.4	+33	6.6	+31	.0
	8	3:34	-2.8 ± 1.6	6.9	33	11.7	31	.5
	9	3:55	1.8 ± 1.6	9.8	6	9.8	66	.3
	10	4:16	-1.8 ± 1.5	10.1	67	10.1	7	.3
	11	4:37	0.7 ± 1.5	10.5	6	10.3	66	.1
	12	4:58	0.4 ± 1.6	10.9	67	10.8	7	.9
11	1	3:45	0.5 ± 1.4	12.9	+10	10.0	+66	.0
	2	4:04	1.6 ± 1.7	10.4	61	13.1	10	1.5
	3	4:23	1.7 ± 1.6	13.5	10	10.6	61	.7
	4	4:40	-2.4 ± 1.6	11.0	61	13.8	10	2.1
	5	4:58	-0.6 ± 1.6	14.1	10	11.3	61	.1
	6	5:17	1.3 ± 1.7	11.5	60	14.4	10	.4
	7	5:32	-4.2 ± 1.5	16.2	47	11.8	19	1.9
	8	5:50	2.8 ± 1.6	12.1	19	16.6	47	.1
	9	6:07	-2.7 ± 1.7	16.8	45	12.4	20	.0
	10	6:25	1.7 ± 1.5	12.8	18	17.1	48	.2
	11	6:43	-4.3 ± 1.6	17.4	46	13.0	20	1.1
	12	7:00	4.1 ± 1.5	13.2	21	17.7	44	.9
12	1	3:08	-1.6 ± 1.4	17.3	+ 9	20.1	+60	1.8
	2	3:28	1.0 ± 1.6	20.5	60	17.6	9	.5
	3	3:46	0.6 ± 1.6	17.9	9	20.8	60	.2
	4	4:04	0.6 ± 1.5	21.1	60	18.2	9	.0
	5	4:22	2.8 ± 1.6	18.5	9	21.4	60	4.2
	6	4:40	-2.7 ± 1.6	21.7	60	18.8	9	4.2
	7	4:57	-2.0 ± 1.6	22.2	25	17.5	39	.5
	8	5:15	2.3 ± 1.6	17.8	39	22.5	25	.1
	9	5:34	-0.1 ± 1.5	22.8	25	18.1	39	3.1
	10	5:52	2.1 ± 1.6	18.4	39	23.1	25	.1
	11	6:10	-5.1 ± 1.5	23.4	25	18.7	39	3.4
	12	6:28	2.6 ± 1.5	19.0	39	23.7	35	.1

13	1	2:18	2.7 ± 1.5	6.8	+32	2.0	+32	.2
	2	2:37	-3.6 ± 1.6	2.4	31	7.2	31	.0
	3	2:56	1.8 ± 1.6	7.5	32	2.7	32	1.0
	4	3:14	-3.6 ± 1.6	3.0	31	7.8	31	.0
	5	3:33	5.7 ± 1.5	8.1	31	3.3	31	2.3
	6	3:51	-2.3 ± 1.6	3.6	31	8.4	31	.5
	7	4:08	-1.5 ± 1.5	7.3	10	4.4	60	3.6
	8	4:26	-2.3 ± 1.5	4.7	60	7.6	9	.4
	9	4:45	2.1 ± 1.6	8.0	10	5.0	60	.1
	10	5:03	-1.7 ± 1.5	5.3	60	8.3	9	.0
	11	5:22	2.2 ± 1.5	8.6	10	5.6	60	.1
	12	5:40	0.2 ± 1.6	5.9	60	8.9	9	1.3
14	1	3:48	-0.8 ± 1.6	13.8	+31	9.1	+31	.1
	2	4:06	-1.2 ± 1.6	9.4	31	14.1	31	1.1
	3	4:27	-0.7 ± 1.6	14.5	31	9.7	31	.0
	4	4:44	1.5 ± 1.6	10.0	31	14.7	31	.1
	5	5:02	0.0 ± 1.7	15.0	30	10.3	32	.6
	6	5:21	-0.2 ± 1.6	10.6	30	15.3	31	1.2
	7	5:39	-0.0 ± 1.7	13.3	5	13.3	65	.2
	8	5:56	3.7 ± 1.6	13.4	66	13.4	6	8.2
	9	6:15	-0.2 ± 1.7	14.0	5	14.0	65	.2
	10	6:32	1.4 ± 1.6	14.0	66	14.0	66	1.6
	11	6:49	-2.4 ± 1.7	14.5	5	14.5	65	2.5
	12	7:05	-1.8 ± 1.6	14.5	66	14.5	6	.8
							χ^2 =	71.0

TABLE 3

Parameters of Cosine Anisotropy:

Flights 8-14 Corrected Data

χ^2/degrees of freedom = 71.0/73, confidence level = 55%

	Best Fit Parameters[a]			Correlation Coefficients		
Celestial Coordinates	amplitude (mK)	R.A. (hours)	dec. (deg.)	(amp,dec)	(amp,R.A.)	(dec,R.A.)
	3.61±0.54	11.23±0.46	19.0±7.5	+0.57	-0.07	+0.06
Galactic Coordinates	amplitude (mK)	l^{II} (deg.)	b^{II} (deg.)	(amp,b)	(amp,l)	(b,l)
	3.61±0.54	229±19	+66.6±6.9	+0.24	-0.56	-0.17
Rectangular[b] Coordinates	T_x(mK)	T_y(mK)	T_z(mK)	(x,y)	(x,z)	(y,z)
	-3.34±0.44	0.68±0.40	1.18±0.49	-0.04	-0.56	-0.01
Diagonalized[c] Coordinates	T_i(mK)	T_j(mK)	T_k(mK)	(i,j)	(i,k)	(j,k)
	3.07±0.59	1.72±0.30	0.80±0.39	0.0	0.0	0.0

[a]Statistical errors have been uniformly increased by 25% to take into account systematic errors as described in text.

[b]Unit vectors point along rectangular celestial coordinate axes. Expressed in celestial coordinates, (hrs. R.A., ^{o}dec.), these unit vectors point along $\hat{x}$ = (0,0^o), $\hat{y}$ = (6,0^o), and $\hat{z}$ = (-, +90^o).

[c]Unit vectors point along axes where errors are uncorrelated. Expressed in celestial coordinates, (hrs. R.A., ^{o}dec.), these unit vectors point along $\hat{i}$ = (11.94, 49.5^o), $\hat{j}$ = (12.5, -39.8^o), and $\hat{k}$ = (6.23, -4.00).

TABLE 4

Fit to Cosine Anisotropy for[a] Alternate Selections of Data

Data Selection	Amplitude (mK)	R.A. (hours)	Dec. (Deg.)	χ^2/DOF	Confidence Level
Flt. 8-14	3.61±0.43	11.23±0.37	19.0±6.0	71.0/73	55%
Flt. 4-11[b]	3.5±0.6	11.0±0.6	6±10	91/77	13%
Flt. 4-11	3.37±0.47	10.57±0.50	5.0±6.6	72.9/67	29%
Flt. 4-14	3.23±0.32	10.95±0.38	13.3±5.3	121.5/103	10%
Flt. 4,6,8 10,12,14	2.51±0.68	11.25±0.72	13.8±10.5	79.3/51	0.5%
Flt. 5,7,9 11,13	3.61±0.54	10.97±0.72	14.8±7.4	39.9/49	82%
Flt. 8-14 uncorrected data[c]	3.4	11.0	16		
Flt. 8-14 roll correction[d]	0.04	13.1	17.1		
Flt. 8-14 galaxy correction[d]	0.13	20.4	-21.5		

[a]Errors quoted in this table are statistical only.

[b]Smoot, Gorenstein, and Muller 1977.

[c]Fit to data with no corrections for aircraft roll, galactic backgrounds, and no subtraction of rotation offset.

[d]Results of cosine fit to corrections only. Inclusion of corrections changes cosine parameters by less than one-standard-deviation.

TABLE 5

Comparison of Dipole Anisotropy Measurements

Reference	Frequency	$\lvert\vec{T}\rvert$	R.A.	Dec.	T_x	T_y	T_z	Correlation Coefficients		
								xy	xz	yz
(1)	(GHz) (2)	(mK) (3)	(hr.) (4)	(°) (5)	(mK) (6)	(mK) (7)	(mK) (8)	(9)	(10)	(11)
Henry (1971)	10.2	3.2 ±0.8	10.5 ±4	-30 ±25						
Corey (1978); Cheng et al. (1979)	19.0	3.1 ±0.7	12.1 ±1.3	-18 ±19	-3.0 ±0.9	-0.1 ±1.0	-1.0 ±1.0	-0.39	-0.44	-0.55
Cheng et al. (1979)	24.8	3.8 ±0.6	12.3 ±0.6	1 ± 9	-3.8 ±0.6	-0.3 ±0.5	0.1 ±0.6	-0.37	0.54	-0.43[a]
Cheng et al. (1979)	31.4	2.4 ±0.4	12.5 ±0.7	3 ±11	-2.4 ±0.4	-0.3 +0.4	0.1 ±0.4	-0.35	0.47	-0.44[a]
This work	33.0	3.6 ±0.5	11.2 ±0.5	19 ±8	-3.4 ±0.4	0.7 ±0.4	1.2 ±0.5	-0.04	-0.56	-0.01

[a]Brian Corey (Private communication).

TABLE 6

Basis Functions for Quadrupole Anisotropy

$\delta \equiv$ Declination, $\alpha \equiv$ Right Ascension

Function	Spherical Harmonic	Angular Dependence
q_1	$\sqrt{\frac{4\pi}{5}}\, Y_{20}$	$\frac{3}{2}\sin^2\delta - \frac{1}{2}$
q_2	$-\sqrt{\frac{16\pi}{15}}\,\frac{Y_{21} - Y_{2-1}}{\sqrt{2}}$	$\sin 2\delta \cos \alpha$
q_3	$-\sqrt{\frac{16\pi}{15}}\,\frac{Y_{21} + Y_{2-1}}{i\sqrt{2}}$	$\sin 2\delta \cos \alpha$
q_4	$\sqrt{\frac{16\pi}{15}}\,\frac{Y_{21} + Y_{2-2}}{\sqrt{2}}$	$\cos^2\delta \cos 2\alpha$
q_5	$\sqrt{\frac{16\pi}{15}}\,\frac{Y_{22} - Y_{2-2}}{i\sqrt{2}}$	$\cos^2\delta \sin 2\alpha$

TABLE 7

Combined Dipole and Quadrupole Model Parameters

Flights 8-14, Northern Hemisphere

	Amplitude (mK)	Error	Correlation Coefficients Matrix						
T_x	-2.3	± 0.7	1.00						
T_y	0.4	0.7	0.12	1.00					
T_z	63.0	29.0	-0.04	-0.29	1.00				
Q_1	40.5	19.0	0.03	0.29	-1.00	1.00			
Q_2	-1.1	0.6	-0.80	-0.34	0.01	0.00	1.00		
Q_3	0.0	0.5	-0.24	-0.68	0.31	-0.31	0.30	1.00	
Q_4	0.1	0.3	0.38	-0.03	-0.30	0.30	-0.23	-0.24	1.00
Q_5	-0.1	0.4	0.12	0.76	-0.09	0.08	-0.42	-0.39	-0.14	1.00

X^2/ Degree of Freedom = 63/68

NOTE — $T(\alpha, \delta) = T_o + T_x\cos\delta\cos\alpha + T_y\cos\delta\sin\alpha + T_z\sin\delta$

$+ Q_1(\frac{3}{2}\sin^2\delta - \frac{1}{2}) + Q_2\sin2\delta\cos\alpha + Q_3\sin2\delta\sin\alpha + Q_4\cos^2\delta\cos2\alpha$

$+ Q_5\cos^2\delta\sin2\alpha$, where $\alpha \equiv$ right ascension, and $\delta \equiv$ declination.

TABLE 8

Measurements of Local Motions

Ref.	Vel. (km/s)	l^{II} (^{o})	b^{II} (^{o})	$\hat{X}$ (km/s)	$\hat{Y}$ (km/s)	$\hat{Z}$ (km/s)	xy	xz	yz
(1)	(2)	(3)	(4)	(5)	(6)	(7)	(8)	(9)	(10)
			Motion of the Sun Relative to the 3K radiation						
This work (A)	361±54	229±19	+67± 7	-94±41	-108±36	330±54	0.06	-0.30	0.32
			Motion of the Sun relative to the Local Group						
Yahil et al. Solution 2. (1977) (B)	308±22	105± 5	-7± 4	-79±28	295±30	-38±24	0.30	0.28	0.51
			Motion of the Local Group relative to the 3K radiation						
			Galactic Coordinates						
(A) - (B)	545±43	268±7	+42±7	-16±50	-404±47	365±59	0.14	-0.17	0.35
			Supergalactic Coordinates						
		24±7	-29±7	-262±58	397±49	-266±49	0.15	0.19	0.41

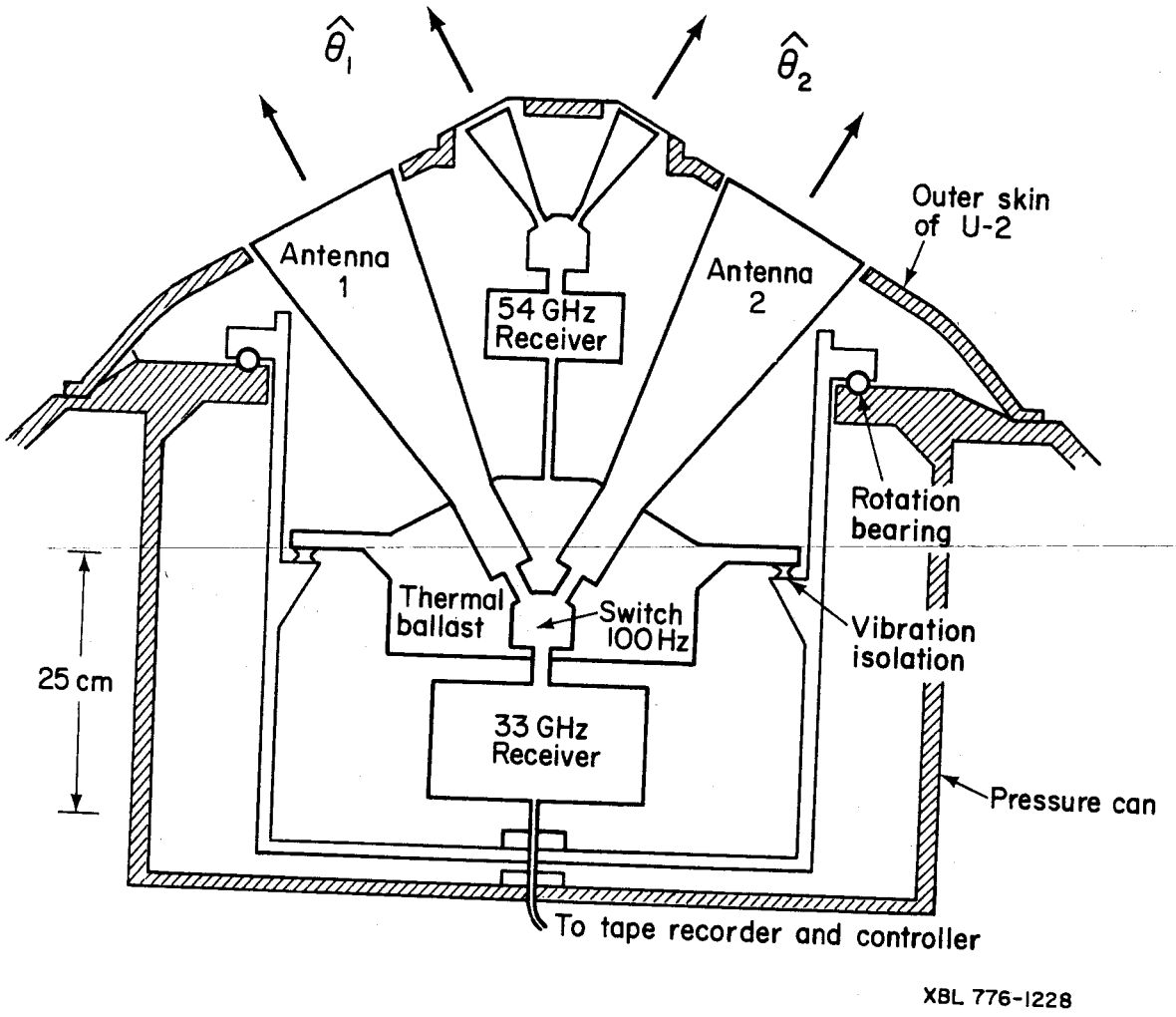

Figure 1: Schematic layout of the radiometer apparatus in the U-2 equipment bay. The main electronics and mechanical components of the system are illustrated. The antennas are shown in the data taking position, with the direction of flight perpendicular to the plane of the drawing. Interchange of the antennas is accomplished by a periodic (once per 64s) rotation of the equipment 180° about the vertical center-line.

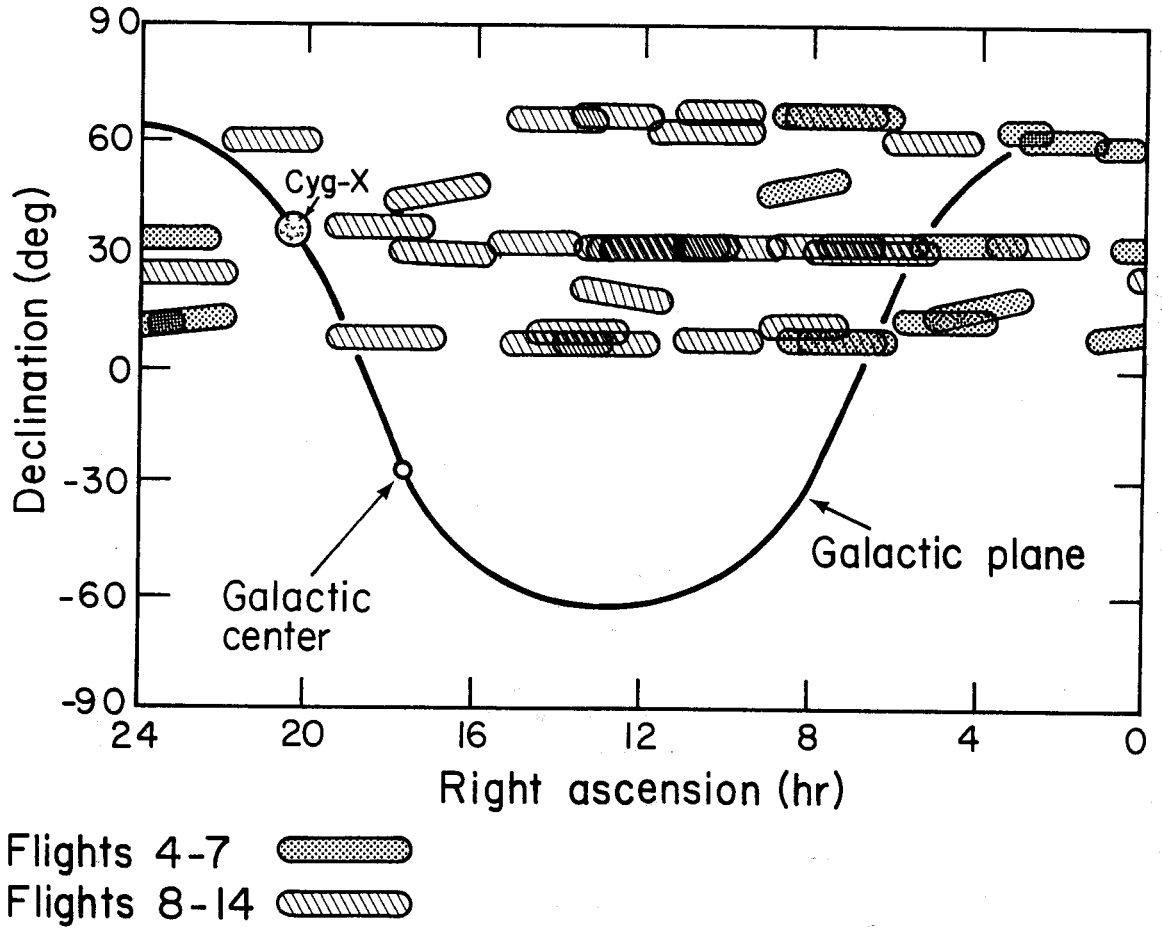

Figure 2: Sky coverage of flights from December 1976 through May 1978. The shaded oval areas consist of four or usually six back-and-forth flight paths. The width of each oval is set by the antenna resolution of 7° FWHM, and the length was set by the rotation of the earth and motion of the U-2.

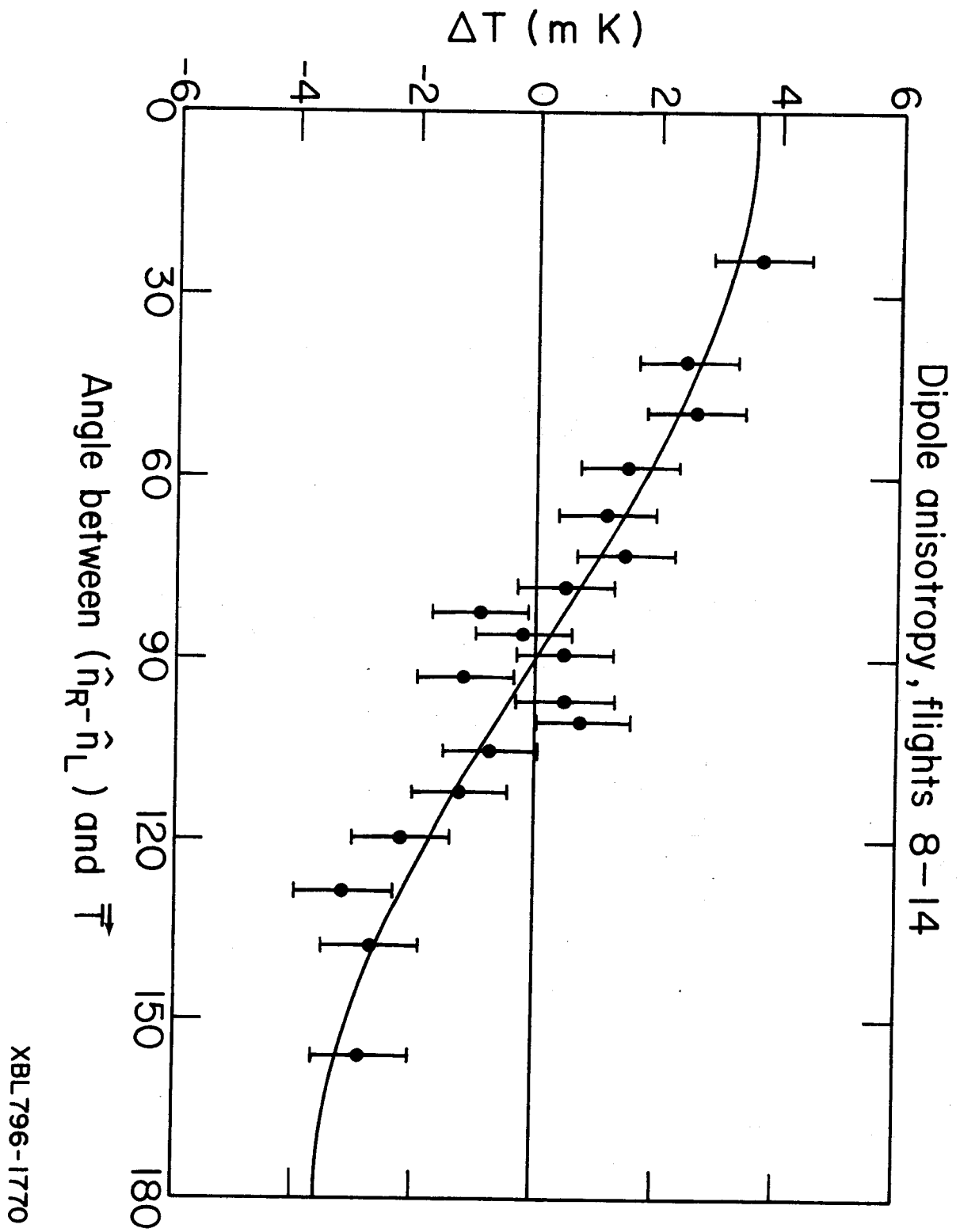

Figure 3: Plot of measured anisotropy versus angle between $(\hat{n}_1-\hat{n}_2)$ and $\vec{T}$. The solid curved line is the best-fit anisotropy $\vec{T}$ = (3.6 mK, 11.2 hours right ascension, 19° declination).

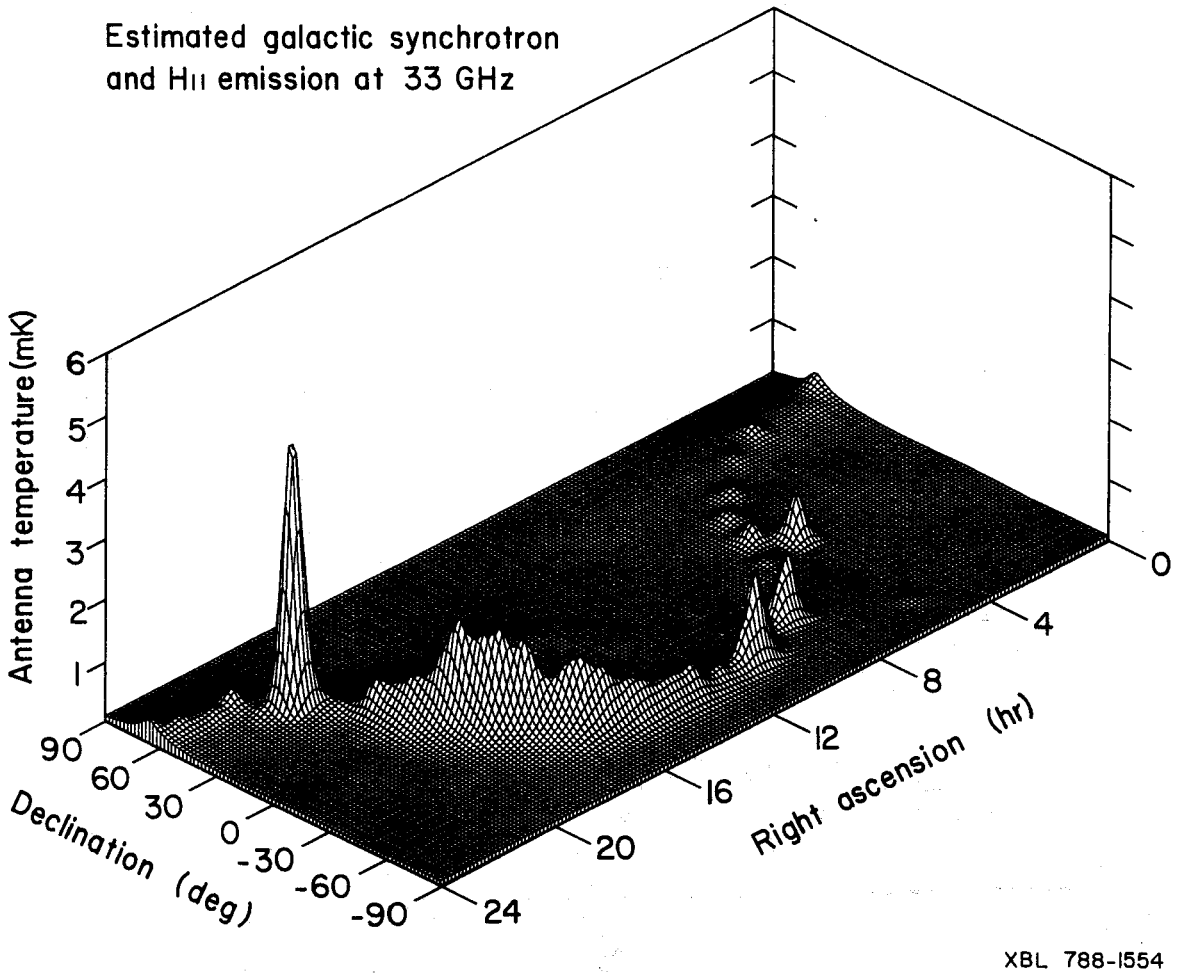

Figure 4: Three dimensional projection of the sum of the contributions of diffuse galactic synchrotron emission and HII-source emission. The HII sources dominate the map and are clearly confined to the galactic plane with the exception of a few significant sources in the Large Magellenic Cloud. The most prominant HII features are the peak on Cygnus-X region and the ridge near the galactic center.

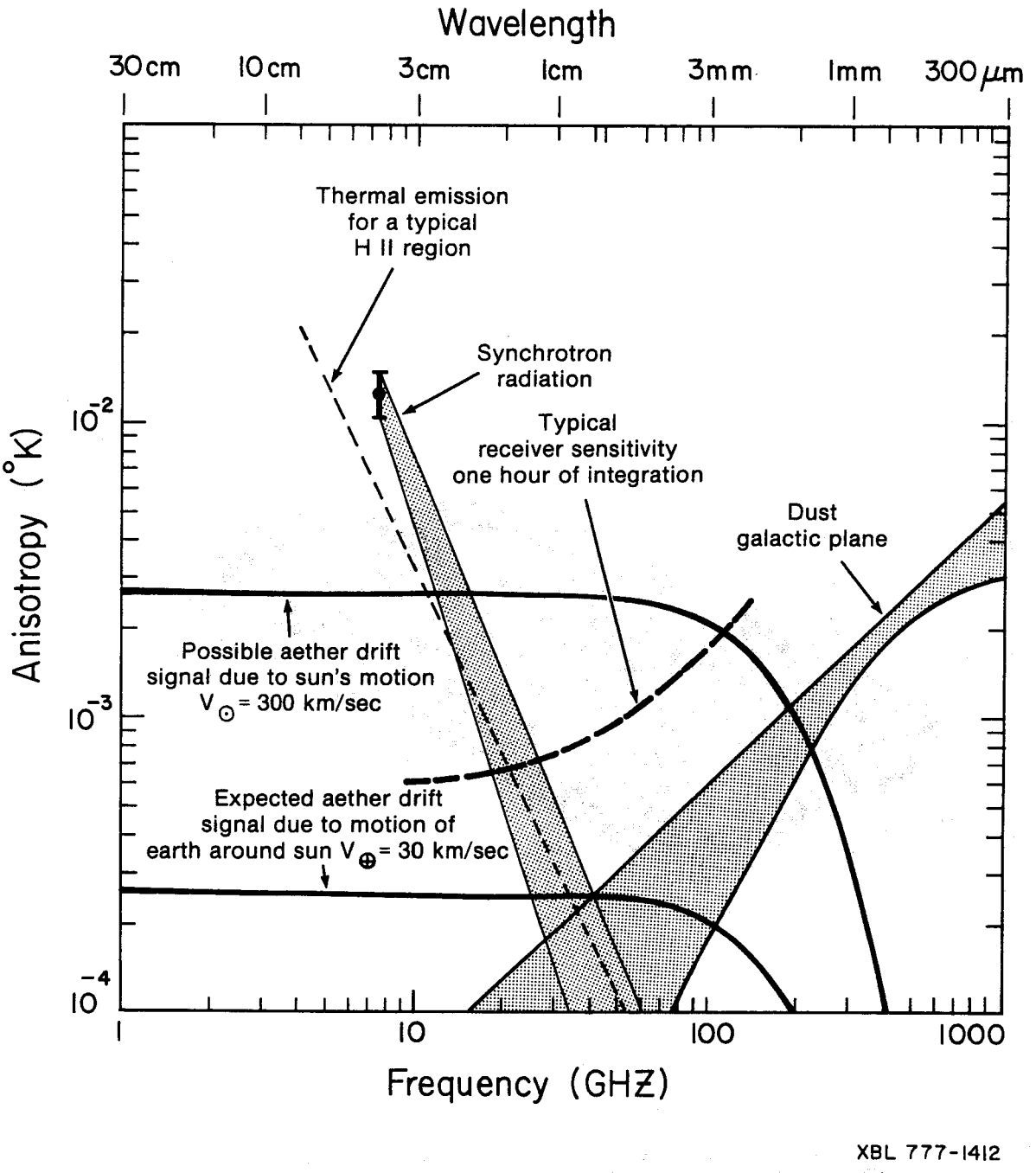

Figure 5: Estimates of galactic radiation backgrounds as a function of frequency. The dust and HII regions are concentrated in the galactic plane and tend to be greatest near the galactic center. Aether drift signals expected due to the solar motion about the galaxy and due to the earth's motion around the sun are included for comparison.

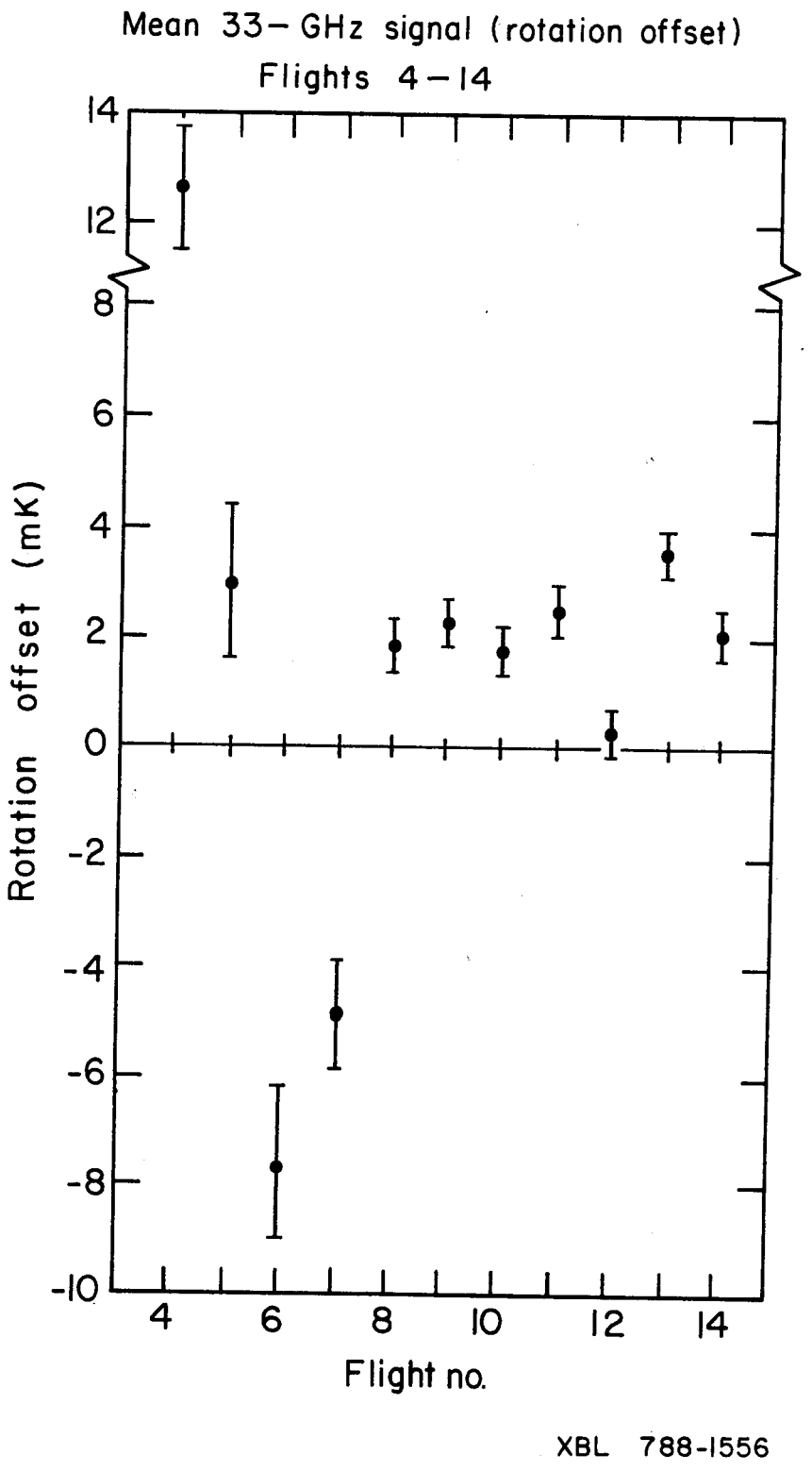

Figure 6: Average 33 GHz rotation-offset as a function of flight number.